Journal of Fluids and Structures (2002) **16**(3), 331–359
doi:10.1006/jfls.2001.0422, available online at http://www.idealibrary.com on IDEAL®

TEMPORAL STABILITY OF FLOW THROUGH VISCOELASTIC TUBES

M. HAMADICHE

Laboratoire de Mécanique des Fluides et d'Acoustique, Ecole Centrale de Lyon
69131 Ecully CEDEX, France

AND

M. GAD-EL-HAK

Department of Aerospace & Mechanical Engineering, University of Notre Dame
Notre Dame, IN 46556, U.S.A.

(Received 22 September 2000, and in final form 20 September 2001)

The stability of the Hagen–Poiseuille flow of a Newtonian fluid in an incompressible, viscoelastic tube contained within a rigid, hollow cylinder is determined using linear stability analysis. The stability of the system subjected to infinitesimal axisymmetric or non-axisymmetric disturbances is considered. The fluid and wall inertia terms are retained in their respective equations of motion. A novel numerical strategy is introduced to study the stability of the coupled fluid–structure system. The strategy alleviates the need for aninitial guess and thus ensures that all the unstable modes within a given closed region in the complex eigenvalue plane will be found. It is found that the system is unstable to both axisymmetric and non-axisymmetric disturbances. Moreover, depending on the values of the control parameters, the first unstable mode can be either an axisymmetric mode with the azimuthal wavenumber $n = 0$ or a non-axisymmetric mode with $n = 1$. For a given azimuthal wavenumber, it is found that there are no more than two unstable modes within the closed region considered here in the complex plane. For both the axisymmetric and non-axisymmetric instabilities, one mode is a solid-based, flow-induced surface instability, while the other one is a fluid-based instability that asymptotes to the least-damped rigid-wall mode as the thickness of the compliant wall tends to zero. All four modes are stabilized, to different degrees, by the solid viscosity.

1. INTRODUCTION

FOR CLOSE TO HALF A CENTURY the science and technology of compliant coatings has fascinated, frustrated and occasionally gratified scientists and engineers searching for methods to delay laminar-to-turbulent flow transition, to reduce skin-friction drag in turbulent wall-bounded flows, to quell vibrations, and to suppress flow-induced noise. Compliant coatings offer the potential for favorable interference with a wall-bounded flow. In its simplest form, the technique is passive, relatively easy to apply to an existing tube or vehicle, and perhaps not too expensive. Unlike other drag reducing techniques such as suction, injection, polymer or particle additives, passive compliant coatings do not require slots, ducts or internal equipment of any kind.

Aside from reducing drag, other reasons for the perennial interest in studying compliant coatings are their many other useful applications, for example as sound absorbent materials

0889–9746/02/030331 + 29 $35.00/0

in noisy flow-carrying ducts in aero-engines, and as flexible surfaces to coat naval vessels for the purposes of shielding their sonar arrays from the sound generated by the boundary-layer pressure fluctuations and of reducing the efficiency of their vibrating metal hulls as sound radiators. An even more important reason to study compliant coatings is the factthat all tubes carrying the bodily fluids of humans and other animals are flexible, and fluid–structure interaction there constitutes a fascinating albeit formidable problem in physics.

1.1. The Present Problem

In this paper, we consider a system where a viscoelastic tube is coupled with a Hagen–Poiseuille flow. The homogeneous, viscoelastic tube is a hollow cylinder surrounded on the outside by a rigid wall, and the basic flow inside the tube is the Hagen–Poiseuille flow in a circular pipe as schematically depicted in Figure 1. We numerically study the stability of the coupled fluid–structure system to infinitesimal axisymmetric or non-axisymmetric disturbances. The fluid and wall inertia terms are retained in the irrespective equations of motion. Both the fluid flow and the compliant wall are considered incompressible.

The stability of Hagen–Poiseuille flow in a rigid circular pipe has been studied by a number of authors including Corcos & Sellars (1959), Davey & Drazin (1969), Salwen & Grosch (1972), Garg & Rouleau (1972) and Gill (1973). They all have concluded that the flow is stable to infinitesimal axisymmetric disturbances as well as to infinitesimal azimuthally varying disturbances. Moreover, they have shown that as the Reynolds number tends to infinity, the wavespeed tends to either unity or to zero with the decay rate satisfying, respectively, $B_m(k\,\mathrm{Re})^{-1/2}$ or $F_m(k\,\mathrm{Re})^{-1/3}$, where B_m and F_m are constants determined by Salwen & Grosch (1972), k is the axial wavenumber, and Re is the Reynolds number.

The stability of Hagen–Poiseuille flow in a compliant circular pipe has been studied by Evrensel *et al.* (1993) and Kumaran (1995*a*), both of whom considered only low-Reynolds-number flows and therefore neglected inertia. Kumaran has shown that the coupled system is unstable to axisymmetric perturbations. Inspection of the energy equation led the author to explain this solid-based instability as being a manifestation of the energy transfer from the mean flow to the disturbance resulting from a discontinuity of the disturbance streamwise velocity at the interface. Kumaran (1995*b*) extended this work to higher Reynolds numbers. He found that the coupled system in this case is stable to axisymmetric disturbances. At high Re, the rate of transport of energy due to the deformation work at the interface is the negative of the rate of transport of energy in the wall layer due to the Reynolds stress $v_r v_x$.

Kumaran (1996) employed a different model for the compliant wall, considered an inviscid flow and developed a stability condition for both axisymmetric and azimuthally

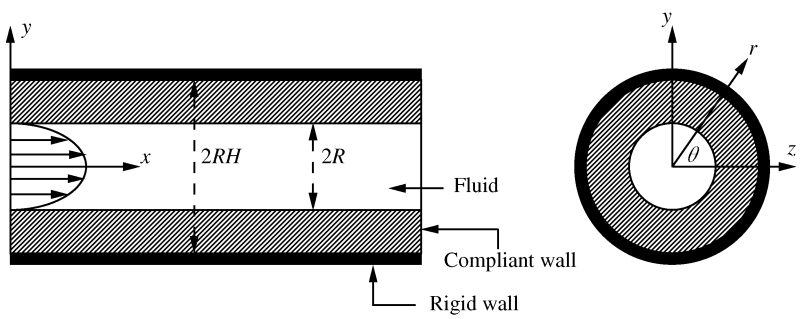

Figure 1. Configuration and definition of coordinate system.

varying disturbances with high azimuthal wavenumbers. The application of this condition to the Hagen–Poiseuille flow showed that the axisymmetric disturbance is stable while the azimuthally varying mode with high wavenumber may be unstable. Additionally, Shankar & Kumaran (1999) considered the stability of nonparabolic flows in flexible tubes.

The stability of the present system for moderate Reynolds numbers to axisymmetric disturbances has been studied by Hamadiche (1997) and Hamadiche & Al-Farkh (1997). They showed that there are two unstable modes. The neutral-stability curves related to these two unstable modes were plotted in the planes formed by the different control parameters of the system. In particular, Hamadiche & Al-Farkh (1997) found that the viscosity of the viscoelastic wall damps those two unstable modes. Kumaran (1998*a*, *b*) has shown, independently, that the system is unstable to axisymmetric disturbances at moderate Reynolds numbers. Very recently, Shankar & Kumaran (2000) extended the latter work to non-axisymmetric disturbances.

Hamadiche (1998) has studied the stability of the coupled system to azimuthally varying disturbances. He showed that such disturbances may be more unstable than axisymmetric ones. Hamadiche (1999*a*, *b*) has examined the energy flux from the fluid to the viscoelastic wall through the interface. A comparison between the total energy flux and the rate of amplification has been made. Hamadiche (1999*a*, *b*) concluded that the mode is unstable/stable when the energy flux is from/to the fluid to/from the wall. Moreover, for low Reynolds numbers, the instability is induced by the work of the streamwise viscous stress, which is in agreement with the earlier conclusion of Kumaran (1998*a*, *b*). However, for high Reynolds numbers, the instability is induced by the work of the forces perpendicular to the wall for both axisymmetric and non-axisymmetric disturbances. Hamadiche (1999*a*, *b*) found that even though the term related to the work of the forces perpendicular to the interface does not contribute to the total variation of the system kinetic energy, it can destabilize it. This observation can be explained as resulting from a redistribution of the kinetic energy in the fluid and the solid: energy in the solid and less energy in the fluid. Consequently, the form of the disturbance may also be modified, which probably leads to a change in the production rate near the wall, thus stabilizing or destabilizing the system according to the sign of the production term.

In the present paper, a numerical method is developed to compute — without a need for an initial guess — all the normal modes of the fluid–structure system within a given closed region in the complex s-plane, where s stands for the complex eigenvalues of the system. The obtained eigenvalues are used as initial values to a Newton–Raphson numerical scheme to converge to more accurate eigenvalues. The continuation method is then used to compute the eigenvalues when the physical parameters of the system vary and to determine the neutral-stability curves. The present strategy was applied successfully to the Hagen–Poiseuille flow in a rigid-walled tube and the obtained eigenvalues were compared with results found in the literature. The numerical strategy was also applied by Hamadiche (1997) to a known case of a viscoelastic-walled tube. The agreement between the results obtained by our method and the results found in the literature is again very good. The present article extends, complements as well as completes the five papers by the first author cited above. It offers new material as well as a single English-language source of the research presented earlier in French.

1.2. Background

The original interest in the field of compliant coatings was spurred by the experiments of Kramer (1957) who demonstrated a coating design based on dolphin's epidermis and claimed substantial transition delay and drag reduction in hydrodynamic flows. Those

experiments were conducted in the seemingly less-than-ideal environment of Long Beach Harbor, CA. Subsequent laboratory attempts to substantiate Kramer's results failed, and the initial interest in the idea faded. A similar bout of excitement and frustration that dealt mostly with the reduction of skin-friction drag in turbulent flows for aeronautical applications followed. Those results were summarized in the comprehensive review by Bushnell *et al.* (1977). During the early 1980s, interest in the subject was rejuvenated, mostly motivated by attempts to improve the performance of underwater vehicles. Significant advances were made during this period in numerical and analytical methods to solve the coupled fluid–structure problem. New experimental tools were developed to measure the minute yet important surface deformation caused by the unsteady fluid forces. Research during this period was reviewed by Gad-el-Hak (1986*a*, 1987, 1996) and Carpenter (1990).

Careful analyses by Carpenter & Garrad (1985), Willis (1986) and Lucey & Carpenter (1995), as well as the well-controlled experiments reported by Willis (1986), Daniel *et al.* (1987) and Gaster (1988) have, for the first time, provided direct confirmation of the transition-delaying potential of compliant coatings, convincingly made a case for the validity of Kramer's original claims, and offered a plausible explanation for the failure of the subsequent laboratory experiments. There is little doubt now that compliant coatings can be *rationally* designed to delay transition and to suppress noise on marine vehicles and other practical hydrodynamic devices. Transition Reynolds numbers that exceed by an order of magnitude those on rigid-surface boundary layers can be readily achieved. The literature on compliant coatings is vast and the reader is referred to the following papers and references therein for more background on the subject: *et al.* (1977), Gad-el-Hak *et al.* (1984), Gad-el-Hak (1986*a*, *b*, 1987, 1996, 2000), Riley *et al.* (1988), Carpenter (1988, 1990, 1993, 1998), Lucey & Carpenter (1993) and Metcalfe (1994). The book by Gad-el-Hak (2000) places compliant coatings within the broader area of flow control.

1.3. System Instabilities

From a fundamental viewpoint, a rich variety of fluid–structure interactions exists when a fluid flows over a surface that is able to interact with the flow. Not surprisingly, instability modes proliferate when two wave-bearing media are coupled. Some waves are flow-based, some are wall-based, and some are a result of the coalescence of both kinds of waves. What is most appealing about compliant coatings is their potential to inhibit, or to foster, the dynamic instabilities that characterize both transitional and turbulent boundary-layer flows, and in turn to modify the mass, heat and momentum fluxes and change the drag and the acoustic properties. While it is relatively easy to suppress a particular instability mode, the challenge is of course to prevent other modes from growing if the aim is, say, to delay laminar-to-turbulent flow transition. From a practical point of view, it is obvious that an in-depth understanding of the coupled system instabilities is a prerequisite for rationally designing a coating that meets a given objective.

There are at least three classification schemes for the fluid–structure waves, each with its own merits. The original scheme is attributable to Landahl (1962) and Benjamin (1963). It divides the waves into three classes according to their response to irreversible energy transfer to and from the compliant wall. Both class A and class B disturbances are essentially oscillations involving conservative energy exchanges between the fluid and solid, but their stability is determined by the net effect of irreversible processes such as dissipation in the coating or energy transfer to the solid by nonconservative hydrodynamic forces. Class A oscillations are Tollmien–Schlichting waves in the boundary layer, modified by the wall compliance, in other words by the motion of the solid in response to the pressure and shear-stress fluctuations in the flow. The disturbance eigenfunction for class A waves has its

maximum amplitude within the fluid region. Such waves are stabilized by the irreversible energy transfer from the fluid to the coating, but destabilized by dissipation in the wall.

Class B waves are found in both the fluid and the wall. However, the disturbance eigenfunction has its maximum amplitude at the fluid–solid interface and thus those waves are principally wall-based modes of instability. Such instability would not exist, had the wall been rigid. The instability is due to the downstream-running free wave in the solid being modified by the fluid loading. The destabilization of class B waves is effected by the phase difference between the pressure perturbation and the wall deformation, which allows a flow of energy from the fluid into the wall. The behavior of Class B waves is the reverse of that for class A waves: stabilized by wall damping but destabilized by the nonconservative hydrodynamic forces. Essentially, class B waves are amplified when the flow supplies sufficient energy to counterbalance the coating's internal dissipation.

Finally, class C waves are akin to the inviscid Kelvin–Helmholtz instability and occur when conservative hydrodynamic forces cause a unidirectional transfer of energy to the solid. The pressure distribution in an inviscid flow over a wavy wall is in exact antiphase with the elevation. In that case, class C waves can grow on the solid surface only if the pressure amplitude is so large as to outweigh the coating stiffness. Class C waves are the result of a modal-coalescence instability where the flow speed is sufficiently high such that the originally upstream-running wall-free-waves are turned to travel downstream and merge with the modified downstream-running wall waves. Irreversible processes in both the fluid and solid have a negligible effect on class C instabilities.

If one considers the total disturbance energy of the coupled fluid–solid system, a decrease in that energy leads to an increase in the amplitude of class A instabilities, class B is associated with an energy increase, and virtually no change in total energy accompanies class C waves. In other words, any nonconservative flow of activation energy from/to the system must be accompanied by disturbance growth of class A/B waves, while the irreversible energy transfer for class C instability is nearly zero.

The second classification scheme is given by Carpenter & Garrad (1985, 1986). It simply divides the waves into fluid-based and solid-based. Tollmien–Schlichting instability (TSI) is an example of fluid-based waves. The solid-based, flow-induced surface instabilities (FISI) are closely analogous to the instabilities studied in hydro- and aeroelasticity, and include both the travelling-wave flutter that moves at speeds close to the solid free-wavespeed (class B) and the essentially static—and more dangerous—divergence waves (class C). The main drawback of this classification scheme is that under certain circumstances, the fluid-based T–S waves and the solid-based flutter can coalesce to form a powerful new instability termed the transitional mode by Sen & Arora (1988). According to the energy criterion advanced by Landahl (1962), this latest instability is a second kind of class C wave. In a physical experiment, however, it is rather difficult to distinguish between static divergence and the transitional mode.

The third scheme to classify the instability waves considers whether they are convective or absolute (Huerre & Monkewitz, 1990). An instability mode is considered to be absolute if there is a pinch point in the Fourier contour, which prevents the temporal amplification rate from being reduced to zero. In this case, the unstable mode propagates upstream as well as downstream and often has a very small (or even zero) group velocity in comparison with the velocity of the mean flow. On the other hand, the unstable development of a disturbance is said to be convective when none of its constituent modes possesses zero group velocity. Both classes A and B are convective, while class C divergence and the transitional modes are absolute. As Carpenter (1990) points out, the occurrence of absolute instabilities would lead to profound changes in the laminar-to-turbulent flow transition process. "It is therefore pointless to consider reducing their growth rate or postponing their appearance to higher

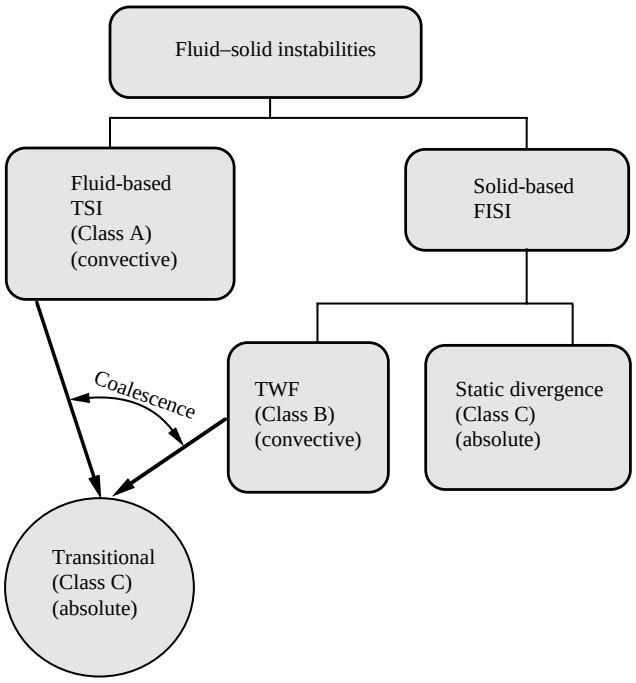

Figure 2. Summary of all three classification schemes of fluid–solid instabilities.

Reynolds number; nothing short of complete suppression would work." Figure 2 combines and summarizes all three classification schemes.

1.4. Outline

In the present study, the stability of the Hagen–Poiseuille flow of a Newtonian fluid in an incompressible, viscoelastic tube contained within a rigid, hollow cylinder is determined using linear stability analysis. The stability of the system subjected to infinitesimal axisymmetric or non-axisymmetric disturbances is considered. A novel numerical method is introduced to study — without a need for an initial guess — the stability of the coupled fluid–structure system.

The paper is organized as follows. Following these introductory remarks, the linearized equations of motion for non-axisymmetric and axisymmetric disturbances are developed in Section 2. The numerical approach and the novel eigenvalue search technique employed here are introduced in Section 3. This is followed in Section 4 by the computed results of the stability of the system to axisymmetric and non-axisymmetric disturbances. Section 5 discusses the energy exchanges between the fluid and the compliant coating. Finally, a discussion of the results and concluding remarks are given in Section 6.

2. PROBLEM FORMULATION

We wish to study the stability of an incompressible, Newtonian fluid of density ρ, viscosity η, and maximum velocity V, flowing in a compliant tube of inner radius R, and outer radius RH. The compliant wall is made of an incompressible, viscoelastic material of density ρ equal to the fluid density, viscosity η_s, and shear modulus G. The pliable material is

surrounded by a rigid wall at the surface $r = RH$, as shown in Figure 1. In the remainder of this paper, dimensionless variables will be used. The length scale is the radius of the tube R, the time scale is $(\rho R^2/G)^{1/2}$, and the velocity scale is $(G/\rho)^{1/2}$. The dimensionless mean flow velocity profile is a Hagen–Poiseuille flow,

$$v = \Gamma(1 - r^2), \tag{1}$$

where $\Gamma = (\rho V^2/G)^{1/2}$. Clearly, Γ is a measure of the relative compliance of the coating since an increase in its value implies a relatively softer material. The governing equations for the fluid are the Navier–Stokes mass and momentum equations:

$$\partial_i v_i = 0, \tag{2}$$

$$\partial_t v_i + v_j \partial_j v_i = -\partial_i p + \varepsilon \Gamma \partial_j^2 v_i, \tag{3}$$

where $\partial_t = \partial/\partial t$, $\partial_j = \partial/\partial x_j$, $\varepsilon = \mathrm{Re}^{-1}$, and $\mathrm{Re} \equiv \rho V R/\eta$ is the Reynolds number. The pressure p in the fluid is nondimensionalized by the shear modulus G. The stress in the fluid is

$$\tau_{ij} = -p\delta_{ij} + \varepsilon \Gamma(\partial_i v_j + \partial_j v_i). \tag{4}$$

The compliant wall of the tube is modelled using the dynamical equations for an incompressible, viscoelastic material (Landau & Lifshitz 1970). The dynamics of the wall is described by a displacement field u_i, which represents the displacement of material points from their steady-state positions dueto the stresses at the interface. For an incompressible material, the displacement field u_i satisfies the solenoidal condition

$$\partial_i u_i = 0, \tag{5}$$

and the momentum conservation equation is

$$\partial_t^2 u_i = -\partial_i p + \partial_j^2 u_i + \varepsilon \Gamma \eta_r \partial_j^2 v_i. \tag{6}$$

The left-hand side represents the rate of change of momentum in a volume element, while the three terms on the right-hand side are, respectively, the divergence of the pressure, the divergence of an elastic stress due to the strain in the material, and the divergence of a viscous stress due to the strain rate. In the latter, the wall velocity is given by $v_i = \partial_t u_i$, and $\eta_r = \eta_s/\eta$. The components of the stress tensor in the solid are given by

$$\sigma_{ij} = -p\delta_{ij} + (\partial_i u_j + \partial_j u_i) + \varepsilon \Gamma \eta_r (\partial_i v_j + \partial_j v_i). \tag{7}$$

Note that the present formulation neglects the effect of pressure gradient along the undisturbed flow on the compliant wall deformation. Owing to this favorable pressure gradient, the deformation would decrease along the tube, thus slightly reducing the effective tube radius R. A variable-radius pipe is a challenging, spatially in homogeneous problem which we defer to another study, and the radius R is taken as constant in the present formulation.

2.1. Non-Axisymmetric Disturbances

In the linear stability analysis, small perturbation in the form of Fourier modes are introduced in the fluid velocity field and the wall displacement field:

$$(v_j, p) = (\tilde{v}_j, \tilde{p}) \mathrm{e}^{(\mathrm{i}kx + \mathrm{i}n\theta + st)} + \mathrm{cc}, \tag{8}$$

$$(u_j, p) = (\tilde{u}_j, \tilde{p}) \mathrm{e}^{(\mathrm{i}kx + \mathrm{i}n\theta + st)} + \mathrm{cc}, \tag{9}$$

where $\tilde{v}_j$ and $\tilde{u}_j$ are the eigenfunctions which are functions of r only, k and n are the axial and the azimuthal wavenumbers, respectively, p is the pressure disturbance, and cc stands for complex conjugate. The real part of the eigenvalue s is the (temporal) growth rate of the perturbation, and the imaginary part is the frequency. Upon inserting the above perturbation velocity (8) into the conservation equations for the fluid velocity field (2) and (3) and neglecting the nonlinear terms in $\tilde{v}_j$, the following equations are obtained for the eigenfunction $\tilde{v}_j$ in cylindrical coordinates:

$$[d_r + r^{-1}]\tilde{v}_r + \mathrm{i}k\tilde{v}_x + \mathrm{i}nr^{-1}\tilde{v}_\theta = 0, \tag{10}$$

$$[s + \Gamma \mathrm{i}k(1 - r^2)]\tilde{v}_r = -d_r\tilde{p} + \varepsilon\Gamma\{[d_r^2 + r^{-1}d_r - r^{-2}(1 + n^2) - k^2]\tilde{v}_r - 2\mathrm{i}nr^{-2}\tilde{v}_\theta\}, \tag{11}$$

$$[s + \Gamma \mathrm{i}k(1 - r^2)]\tilde{v}_x - 2\Gamma r\tilde{v}_r = -\mathrm{i}k\tilde{p} + \varepsilon\Gamma[d_r^2 + r^{-1}d_r - (k^2 + n^2r^{-2})]\tilde{v}_x, \tag{12}$$

$$[s + \Gamma \mathrm{i}k(1 - r^2)]\tilde{v}_\theta = -\mathrm{i}n\tilde{p}r^{-1} + \varepsilon\Gamma\{[d_r^2 + r^{-1}d_r - r^{-2}(1 + n^2) - k^2]\tilde{v}_\theta + 2\mathrm{i}nr^{-2}\tilde{v}_r\}, \tag{13}$$

where d_r stands for derivative with respect to r, and $\tilde{p}(r)$ is the eigenfunction for the pressure.

Similarly, the equations for the eigenfunction $\tilde{u}_j$ can be obtained by inserting the equation for the solid displacement perturbation (9) into the conservation equations (5) and (6), yielding cylindrical coordinates

$$[d_r + r^{-1}]\tilde{u}_r + \mathrm{i}k\tilde{u}_x + \mathrm{i}nr^{-1}\tilde{u}_\theta = 0, \tag{14}$$

$$s^2\tilde{u}_r = -d_r\tilde{p} + (1 + \varepsilon\Gamma\eta_r s)\{[d_r^2 + r^{-1}d_r - r^{-2}(1 + n^2) - k^2]\tilde{u}_r - 2\mathrm{i}nr^{-2}\tilde{u}_\theta\}, \tag{15}$$

$$s^2\tilde{u}_x = -\mathrm{i}k\tilde{p} + (1 + \varepsilon\Gamma\eta_r s)[d_r^2 + r^{-1}d_r - (k^2 + n^2r^{-2})]\tilde{u}_x, \tag{16}$$

$$s^2\tilde{u}_\theta = -\mathrm{i}nr^{-1}\tilde{p} + (1 + \varepsilon\Gamma\eta_r s)\{[d_r^2 + r^{-1}d_r - r^{-2}(1 + n^2) - k^2]\tilde{u}_\theta + 2\mathrm{i}nr^{-2}\tilde{u}_r\}. \tag{17}$$

The boundary conditions at the center of the tube $r = 0$, applied to the azimuthally varying modes with azimuthal wavenumber $n = 1$, are

$$\tilde{v}_r + \mathrm{i}\tilde{v}_\theta = 0, \qquad \tilde{v}_x = \tilde{p} = 0, \tag{18, 19}$$

at the interface $r = 1$

$$\tilde{v}_r = s\tilde{u}_r, \qquad \tilde{v}_x - 2\Gamma\tilde{u}_r = s\tilde{u}_x, \qquad \tilde{v}_\theta = s\tilde{u}_\theta, \tag{20, 21, 22}$$

$$\tilde{\sigma}_{rr} = \tilde{\tau}_{rr}, \quad \tilde{\sigma}_{r\theta} = \tilde{\tau}_{r\theta}, \quad \tilde{\sigma}_{rx} = \tilde{\tau}_{rx}, \tag{23}$$

and at the surface $r = H$

$$\tilde{u}_r = 0, \quad \tilde{u}_\theta = 0, \quad \tilde{u}_x = 0. \tag{24}$$

The term $-2\Gamma\tilde{u}_r$ in equation (21) represents the variation of the mean velocity at the interface due to the surface displacement.

The boundary conditions at $r = 0$, applied to the two components of non-axisymmetric eigenmodes ($\tilde{v}_r$, $\tilde{v}_\theta$) with azimuthal wavenumber $n > 1$, are

$$\tilde{v}_r = \tilde{v}_\theta = 0, \tag{25}$$

the remaining boundary conditions are identical to those applied to the eigenmodes with azimuthal wavenumber $n = 1$.

The stress tensor components in equation (23) are

$$\tilde{\tau}_{rr} = -\tilde{p} + 2\varepsilon\Gamma(d_r\tilde{v}_r), \tag{26}$$

$$\tilde{\tau}_{rx} = (\varepsilon\Gamma)(d_r\tilde{v}_x + \mathrm{i}k\tilde{v}_r), \tag{27}$$

$$\tilde{\tau}_{r\theta} = \varepsilon\Gamma(\mathrm{i}nr^{-1}\tilde{v}_r + d_r\tilde{v}_\theta - r^{-1}\tilde{v}_\theta), \tag{28}$$

$$\tilde{\sigma}_{rr} = -\tilde{p} + 2(1 + \varepsilon\Gamma\eta_r s)d_r\tilde{u}_r, \tag{29}$$

$$\tilde{\sigma}_{rx} = (1 + \varepsilon\Gamma\eta_r s)(d_r\tilde{u}_x + \mathrm{i}k\tilde{u}_r), \tag{30}$$

$$\tilde{\sigma}_{r\theta} = \varepsilon\Gamma(\mathrm{i}nr^{-1}\tilde{u}_r + d_r\tilde{u}_\theta - r^{-1}\tilde{u}_\theta). \tag{31}$$

The linearized mass and momentum equations for the fluid and solid can be transformed into a system of first-order differential equations. In order to do that, we take the derivative with respect to r of all the terms in the continuity equations (10) and (14). This yields

$$[d_r^2 + r^{-1}d_r - r^{-2}]\tilde{v}_r + \mathrm{i}kd_r\tilde{v}_x + \mathrm{i}nd_r(r^{-1}\tilde{v}_\theta) = 0, \tag{32}$$

$$[d_r^2 + r^{-1}d_r - r^{-2}]\tilde{u}_r + \mathrm{i}kd_r\tilde{u}_x + \mathrm{i}nd_r(r^{-1}\tilde{u}_\theta) = 0. \tag{33}$$

equations (32) and (33) give $d_r^2\tilde{v}_r$ and $d_r^2\tilde{u}_r$ as functions of the velocity and displacement components and their first-order derivatives. If these functions are substituted into equations (11) and (15), the system can be transformed into the following first-order differential equations, first for the fluid:

$$d_r\tilde{v}_r = -r^{-1}v_r - \mathrm{i}k\tilde{v}_x - \mathrm{i}nr^{-1}\tilde{v}_\theta, \tag{34}$$

$$d_r\tilde{p} = -[s + \Gamma\mathrm{i}k(1 - r^2)]\tilde{v}_r - \varepsilon\Gamma\{(r^{-2}n^2 + k^2)\tilde{v}_r + \mathrm{i}nr^{-2}\tilde{v}_\theta + \mathrm{i}k\tilde{\xi}_x + \mathrm{i}nr^{-1}\tilde{\xi}_\theta\}, \tag{35}$$

$$d_r\tilde{\xi}_x = -r^{-1}\tilde{\xi}_x + (k^2 + n^2r^{-2})\tilde{v}_x + (\varepsilon\Gamma)^{-1}[s + \Gamma\mathrm{i}k(1 - r^2)]\tilde{v}_x - 2\varepsilon^{-1}r\tilde{v}_r + \mathrm{i}k(\varepsilon\Gamma)^{-1}\tilde{p}, \tag{36}$$

$$d_r\tilde{v}_x = \tilde{\xi}_x, \tag{37}$$

$$d_r\tilde{\xi}_\theta = -r^{-1}\tilde{\xi}_\theta + [r^{-2}(1 + n^2) + k^2]\tilde{v}_\theta - 2\mathrm{i}nr^{-2}\tilde{v}_r + (\varepsilon\Gamma)^{-1}[s + \Gamma\mathrm{i}k(1 - r^2)]\tilde{v}_\theta + \mathrm{i}n(r\varepsilon\Gamma)^{-1}\tilde{p}, \tag{38}$$

$$d_r\tilde{v}_\theta = \tilde{\xi}_\theta, \tag{39}$$

and the following first-order differential equations for the compliant solid:

$$d_r\tilde{u}_r = -r^{-1}u_r - \mathrm{i}k\tilde{u}_x - \mathrm{i}nr^{-1}\tilde{u}_\theta, \tag{40}$$

$$d_r\tilde{p} = -s^2\tilde{u}_r - (1 + \varepsilon\Gamma\eta_r s)\{(r^{-2}n^2 + k^2)\tilde{u}_r + \mathrm{i}nr^{-2}\tilde{u}_\theta + \mathrm{i}k\tilde{\chi}_x + \mathrm{i}nr^{-1}\tilde{\chi}_\theta\}, \tag{41}$$

$$d_r\tilde{\chi}_x = -r^{-1}\tilde{\chi}_x + (k^2 + n^2r^{-2})\tilde{u}_x + (1 + \varepsilon\Gamma\eta_r s)^{-1}s^2\tilde{u}_x + \mathrm{i}k(1 + \varepsilon\Gamma\eta_r s)^{-1}\tilde{p}, \tag{42}$$

$$d_r\tilde{u}_x = \tilde{\chi}_x, \tag{43}$$

$$d_r\tilde{\chi}_\theta = -r^{-1}\tilde{\chi}_\theta + [r^{-2}(1 + n^2) + k^2]\tilde{u}_\theta - 2\mathrm{i}nr^{-2}\tilde{u}_r + (1 + \varepsilon\Gamma\eta_r s)^{-1}[s^2\tilde{u}_\theta + \mathrm{i}nr^{-1}\tilde{p}], \tag{44}$$

$$d_r\tilde{u}_\theta = \tilde{\chi}_\theta, \tag{45}$$

where the vectors $(\xi_r, \xi_\theta, \xi_x)$ and $(\chi_r, \chi_\theta, \chi_x)$ are, respectively, the derivatives of (v_r, v_θ, v_x) and (u_r, u_θ, u_x) with respect to r.

2.2. Axisymmetric Disturbances

To study the temporal stability of the coupled system to axisymmetric disturbances, small perturbation in the form of axisymmetric Fourier modes are introduced in the fluid velocity field and the wall displacement field. These read, respectively, as

$$v_i = \tilde{v}_i e^{(ikx+st)} + \text{cc}, \tag{46}$$

$$u_i = \tilde{u}_i e^{(ikx+st)} + \text{cc}. \tag{47}$$

The first-order differential equations related to axisymmetric disturbances can readily be obtained by inserting $n = 0$, $\tilde{v}_\theta = 0$, and $\tilde{u}_\theta = 0$ into equations (34)–(45). The corresponding boundary conditions read as follows:
at the center of the tube, $r = 0$,

$$\tilde{v}_r = 0, \quad d_r \tilde{v}_x = 0, \tag{48}$$

at the interface, $r = 1$,

$$\tilde{v}_r = s\tilde{u}_r, \quad \tilde{v}_x - 2\Gamma\tilde{u}_r = s\tilde{u}_x, \tag{49}$$

$$\tilde{\sigma}_{rr} = \tilde{\tau}_{rr}, \quad \tilde{\sigma}_{rx} = \tilde{\tau}_{rx}, \tag{50}$$

and at the surface, $r = H$,

$$\tilde{u}_r = 0, \quad \tilde{u}_x = 0. \tag{51}$$

3. NUMERICAL METHOD

Differential equations (34)–(39) and their equivalents for the axisymmetric disturbances were solved using a fourth-order Runge–Kutta method to arrive at three independent solutions $(\mathbf{X}_1, \mathbf{X}_2, \mathbf{X}_3)$ each of which satisfy the boundary conditions at $r = 0$. The independence of the three solutions is ensured by starting the computation with one of the three independent vectors formed by several values of the vector $(\xi_r, \xi_\theta, \xi_x)$ at $r = 0$. The chosen values must form a free set of vectors. Then the general solution in the fluid is

$$\mathbf{Z}_1 = A_1\mathbf{X}_1 + A_2\mathbf{X}_2 + A_3\mathbf{X}_3, \tag{52}$$

where (A_1, A_2, A_3) are arbitrary constants.

Similarly, for the displacement field in the solid, we obtain three independent solutions $(\mathbf{Y}_1, \mathbf{Y}_2, \mathbf{Y}_3)$ each of which satisfy the boundary conditions at $r = H$. The independence of the solutions is also ensured by beginning the computation with one of the three independent values of the vector $(\chi_r, \chi_\theta, \chi_x)$ at $r = H$. The general solution in the solid medium is

$$\mathbf{Z}_2 = B_1\mathbf{Y}_1 + B_2\mathbf{Y}_2 + B_3\mathbf{Y}_3, \tag{53}$$

where (B_1, B_2, B_3) are arbitrary constants. The boundary conditions at $r = 1$ lead to the eigenvalue problem

$$\mathbf{M}\,\mathbf{C} = 0, \tag{54}$$

where the elements of the 6×6 matrix $\mathbf{M}$ are a linear combination of the particular solution components $(\mathbf{X}_1, \mathbf{X}_2, \mathbf{X}_3)$, $(\mathbf{Y}_1, \mathbf{Y}_2, \mathbf{Y}_3)$ and their derivatives with respect to r at $r = 1$, which involve k, n, Re, H, η_r and Γ. The components of the vector $\mathbf{C}$ are the six arbitrary constants $A_1, A_2, A_3, B_1, B_2, B_3$.

The characteristic equation is obtained by setting the determinant of the characteristic matrix **M** to zero. In order to use the continuation method, the derivative with respect to s of the determinant of the matrix **M** is computed, where s is the complex eigenvalue of the coupled system. For this, the derivative with respect to s of the linearized mass and momentum equations is needed which leads to another system of first-order differential equations. The resulting system is solved using a fourth-order Runge–Kutta scheme. This leads to the derivative with respect to s of the elements of the matrix **M** which gives the derivative of the determinant of **M**. The solution of the characteristic equation gives the growth rate as a function of the Reynolds number for different values of the parameters k, n, H, η_r and Γ. The effects of changes in the parameter values on the system stability are examined in Sections 4.1 and 4.2 for, respectively, the axisymmetric and non-axisymmetric disturbances.

3.1. Eigenvalue Search Technique

The method proposed by Garg & Rouleau (1972) to compute the number of poles of a complex function lying within a closed curve is extended in this paper to determine all the singularities of a complex function lying within a closed region in the complex eigenvalue plane. Let $f(z)$ be the determinant of the matrix **M**. This function is *a priori* assumed, and later verified, to be analytic. Cauchy's theorem gives

$$2\pi\mathrm{i}(N - P) = \oint_C \frac{\partial_z f(z)}{f(z)}\,\mathrm{d}z, \tag{55}$$

where N and P denote, respectively, the number of zeros and the number of poles of the function $f(z)$ — counted with their multiplicity — within the closed region C. Since the determinant is an analytic function of the complex eigenvalue s, we have

$$\oint_C f(z)\,\mathrm{d}z = 0, \tag{56}$$

so that $P = 0$. In our computation, the curve C is a circle centered on the origin of the complex z-plane. Knowing the number of zeros of the determinant N which is the number of eigenmodes, we can use Cauchy's theorem and the theorem of the residue to evaluate the sum of eigenvalues as well as the sum of their jth power inside the closed region C. Thus,

$$2\pi\mathrm{i}\sum z_m^j = \oint_C z^j \frac{\partial_z f(z)}{f(z)}\,\mathrm{d}z, \tag{57}$$

where the sum is over the suffix m, $1 \leq m \leq N$, the exponent j is held constant, and z_m is the value of the complex variable z in the pole m, which is the desired eigenvalue. Having the number of zeros N from equation (55), equation (57) gives N nonlinear equations which in principle allows us to determine the eigenvalues. The solution of such a system is, however, very difficult to obtain when N is large. In order to avoid this difficulty, the diameter of the circle C is first defined in such a way that the number of zeros $N \leq 3$, which is the maximum degree of a polynomial that can be solved analytically. Having the previous eigenvalues, the diameter of the circle can now be increased to add not more than three new eigenvalues. The newly obtained nonlinear system from equation (57) is transformed again into a polynomial of a degree equal to the number of the added eigenvalues. The resulting polynomial can then be solved to give new eigenvalues, and so on until a value of the diameter C is reached beyond which all the added modes have a high amplification rate, high frequency, or both.

Such spurious modes are not of physical significance and one may ignore them. When the desired value of the diameter is reached, an iterative technique is used in order to eliminate the cut-off error and to converge to the exact eigenvalues. The continuation method then permits the computation of the eigenvalues for other values of the wall and fluid parameters.

Note that in the method used by Garg & Rouleau (1972), the examined region has to be very small for the iterative process to converge. In the present method, we compute the exact values of the eigenmodes in the examined region where the number of modes does not exceed three. The area examined is not necessarily small and the iterative process is used only to eliminate the cut-off error.

It is also noted that the eigenvalue search technique developed here is more efficient and does not produce spurious modes as occasionaly encountered when using the classical QZ search technique used by, for example, Yeo *et al.* (1996) to study the absolute instability of a boundary layer flow over a viscoelastic wall. In contrast to the 6×6 matrix resulting from our search strategy, the QZ search technique results in a matrix size of the order of $4N$, where N is the number of discrete points in the physical space.

In order to validate our method, it was used to find the least-damped disturbance to Poiseuille flow in a circular, rigid-walled pipe, previously obtained by Gill (1973). The agreement between Gill's results and the present method is excellent, and that agreement is true for both axisymmetric and non-axisymmetric, temporally damped as well as spatially decaying disturbances.

As the no-displacement conditions are applied at $r = H$, it is expected that the system described behaves like a rigid-walled tube when the depth of the viscoelastic material is small in comparison with the radius of the tube. Figure 3 displays the rate of amplification (s_r) and the wavespeed (s_i) of the least-damped modes obtained by the present method with $H = 1{\cdot}05$. The same figure shows a comparison with the Salwen & Grosch (1972) numerical calculations in a rigid-walled tube for the azimuthal wavenumbers $n = 1, 2, 3, 4$. The values of the amplification rate and the wavespeed for the rigid tube were computed from the Salwen and Grosch formulas recalled in Section 1.1. The agreement between the present method and their results is excellent when the Reynolds number is high, where the formulas are expected to be accurate. The discrepancy observed at low Reynolds numbers is likely

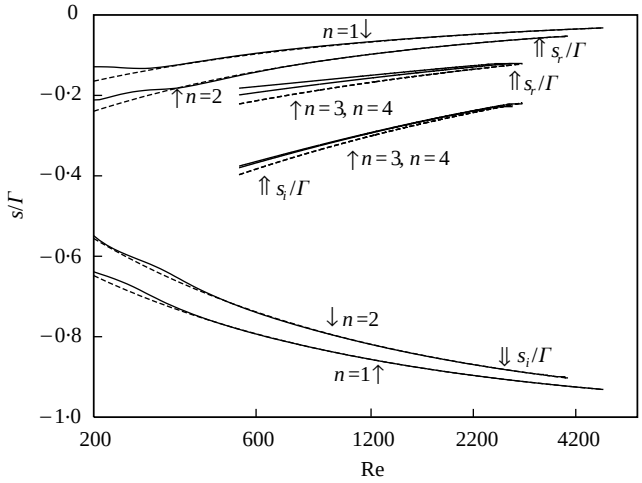

Figure 3. Comparison of the real and imaginary parts of s/Γ with the Salwen and Grosch results; $H = 1{\cdot}05$, $k = 1$, $\Gamma = 7$, $\eta_r = 0$: ——, our results; – – –, Salwen & Grosch (1972).

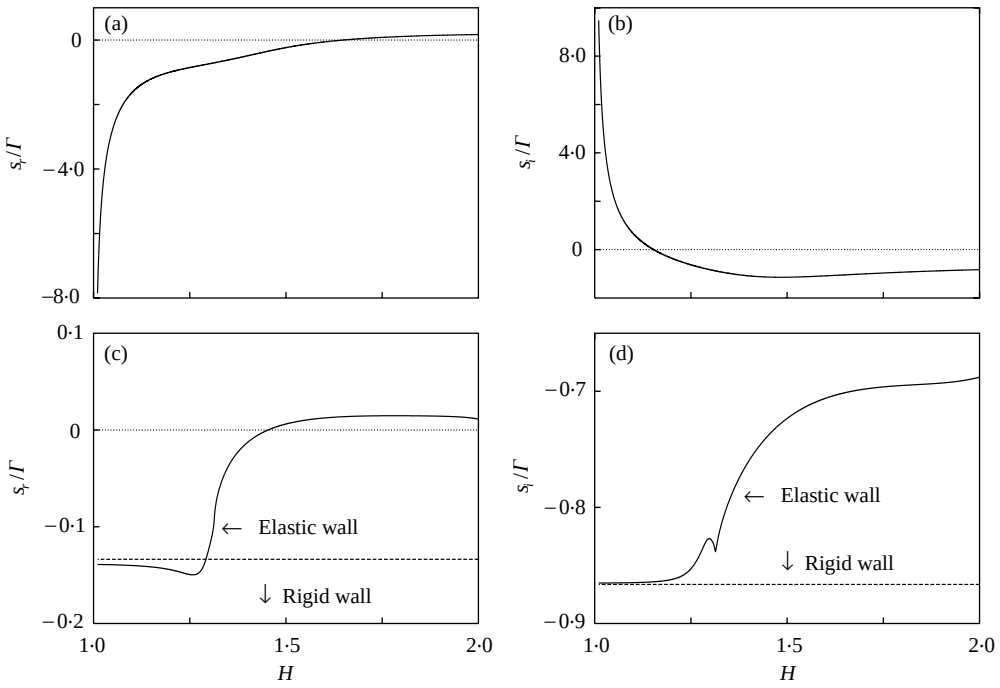

Figure 4. Real and imaginary parts of s/Γ for the axisymmetric unstable modes versus the depth of the elastic material; $\Gamma = 6$, $n = 0$, $\eta_r = 0$. (a) Mode I real part; $k = 2{\cdot}5$, Re $= 23$. (b) Mode I imaginary part; $k = 2{\cdot}5$, Re $= 23$. (c) Mode II real part; $k = 1$, Re $= 450$. (d) Mode II imaginary part; $k = 1$, Re $= 450$.

due to the failure of the Salwen and Grosch formulas in this regime. Moreover, as will be discussed in the following section, Figures 4 and 9 show the limits of the amplification rate and the wavespeed of, respectively, the axisymmetric and non-axisymmetric modes when the depth of the viscoelastic material goes to zero ($H \to 1$). The figures also show a comparison with the rigid-tube results given by the Salwen and Grosch formulas. As can be seen, the agreement between the present Mode II and Mode IV results† and the rigid-tube results is good.

A comparison with the solution obtained by Kumaran (1995*a*) for the Hagen–Poiseuille flow in a viscoelastic tube has been made in Hamadiche & Al-Farkh (1997). The agreement between the results of the present numerical approach and the results of Kumaran was found to be of the same order as the algorithm round-off error.

4. RESULTS

4.1. Stability of Axisymmetric Disturbances

For all the wall and fluid parameters explored here in the closed region in the complex s-plane, we do not find more than two unstable axisymmetric modes, which we term Mode I and Mode II. The axisymmetric unstable Mode I is strongly stable for $H < 1{\cdot}7$, and

† Four different instability modes are identified in the present study. These will be discussed in the following section.

diverges§ when the depth of the viscoelastic material tends to zero, as can be seen in Figure 4(a). For $H > 1{\cdot}7$, Mode I is weakly unstable. At small values of H, Mode I wavespeed is much larger than 1, as can be seen in Figure 4(b). Recalling that the rigid-walled tube result of Salwen & Grosch (1972) gives a wavespeed that tends to either unity or zero as the Reynolds number $\mathrm{Re} \to \infty$, it then follows that Mode I instability does not exist in rigid tubes, and is due to the viscoelastic wall. According to Carpenter and Garrad (1985), this is a solid-based, flow-induced surface instability.

The second axisymmetric unstable mode, Mode II, is identified with the least-damped mode in the rigid-walled tube when the depth of the viscoelastic coating goes to zero, as shown in Figure 4(c,d). This is then a fluid-based instability according to the classification scheme of Carpenter & Garrad (1985) described in Section 1.3. The kink in Figure 4(d) was carefully examined and the curve in its vicinity is in fact continuous. Therefore, this kink is a mere indication of rapid variation in the wavespeed with the coating thickness and is not a result of bifurcation or mode jumping in the numerical scheme.

The neutral-stability curves in the planes (Γ, Re) and (k, Re) are very complex as has been shown by Hamadiche & Al-Farkh (1997). Figures 5 and 6 show examples of, respectively, Mode I and Mode II neutral-stability curves in the plane (k, Re) for several values of Γ. The axisymmetric Mode I becomes stable at high Reynolds number as the asymptotic analysis of Kumaran (1995b) and the numerical results of Hamadiche (1999*a*) have shown. The effect of moderately increasing the Reynolds number is to not only stabilize Mode I for all values of Γ examined, as shown in Figure 5, but also to increase the instability of the second axisymmetric Mode II for $\Gamma = 4$ and 6, as shown in Figure 6. For $\Gamma = 8$, the k-range of Mode II instability actually decreases with Reynolds number increase.

Note that the system is unstable at low Reynolds numbers when the shear modulus is sufficiently small. This may be explained by the fact that the energy needed to destabilize the system is very small when the coating is sufficiently soft. In the region labelled "not explored" in Figures 5 and 6, a new unstable region may exist, as has been shown by Hamadiche & Al-Farkh (1997).

At low Re, the effect of decreasing the depth of the viscoelastic material is to stabilize the system as shown for Mode I instability in Figure 7. As expected, the system is stable when the depth of the viscoelastic material goes to zero. Note that only long-wave (low-wavenumber) instability persists when the Reynolds number and the coating thickness increase. In Figure 8, we plot, for both Mode I and Mode II, typical radial profiles for the disturbance velocity and stress. Each profile extends from the pipe centerline to the interface between the compliant coating and the rigid wall. We observe that the important motion is in the axial direction and that the disturbance inside the fluid medium is almost constant. More importantly, the energy production by the Reynolds stress, $-v_r v_x \, \mathrm{d}v/\mathrm{d}r$, is negative for Mode I and positive for Mode II† as can be seen in Figure 8(a) and 8(b), respectively. Therefore, the Reynolds stress tends to stabilize Mode I disturbance but destabilize Mode II, even though both modes are unstable under the conditions considered in this figure. As will be shown in Section 5, the energy disturbance production for Mode I is done by the work of the viscous shear stress at the interface. Of note is the position of the disturbance peak amplitude. For the solid-based Mode I, this occurs at the fluid–solid interface much like the travelling-wave flutter eigenfunction described by Carpenter & Gajjar (1990). The modified rigid-pipe Mode II, on the other hand, has its peak amplitude occurring in the flow.

§ Not to be confused with static-divergence waves. Mode I becomes extremely stabilized as the coating thickness goes to zero.

† For Mode II, the Reynolds stress $v_r v_x$ is large and positive near the wall, but changes sign and diminishes far from the fluid–solid interface.

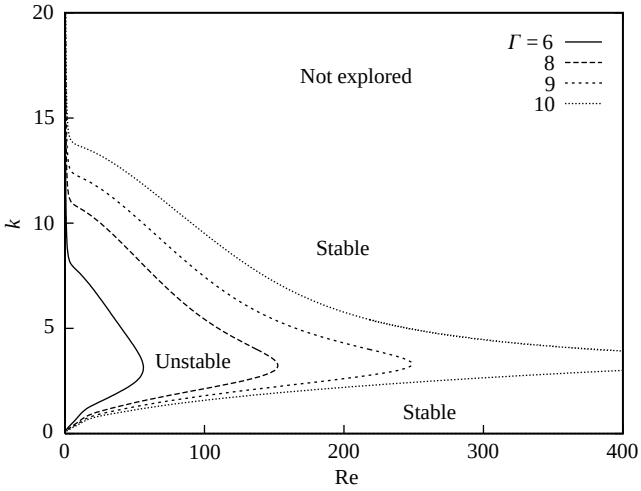

Figure 5. Neutral-stability curves in the (k, Re) plane for several values of Γ. Mode I instability; $H = 2$, $\eta_r = 0$, $n = 0$.

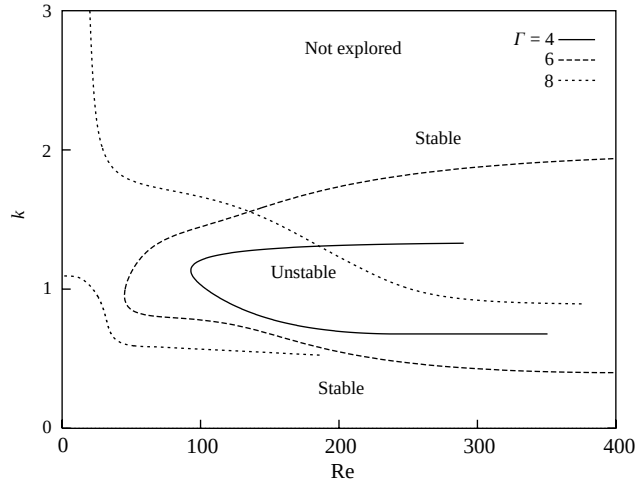

Figure 6. Neutral-stability curves in the (k, Re) plane for several values of Γ. Mode II instability; $H = 2$, $\eta_r = 0$, $n = 0$.

4.2. Stability of Non-Axisymmetric Disturbances

For all the wall and fluid parameters explored here in the closed region in the complex s-plane, we do not find more than two unstable non-axisymmetric modes for each value of the azimuthal wavenumber n. For $n = 1$, we term the corresponding modes Mode III and Mode IV. The non-axisymmetric Mode III becomes extremely stabilized when the depth of the viscoelastic material goes to zero as shown in Figure 9(a). This is a solid-based, flow-induced surface instability. The second non-axisymmetric unstable mode, Mode IV, is identified with the least-damped mode in the rigid-walled tube when the depth of the viscoelastic coating goes to zero, as shown in Figure 9(c,d). This is a fluid-based instability.

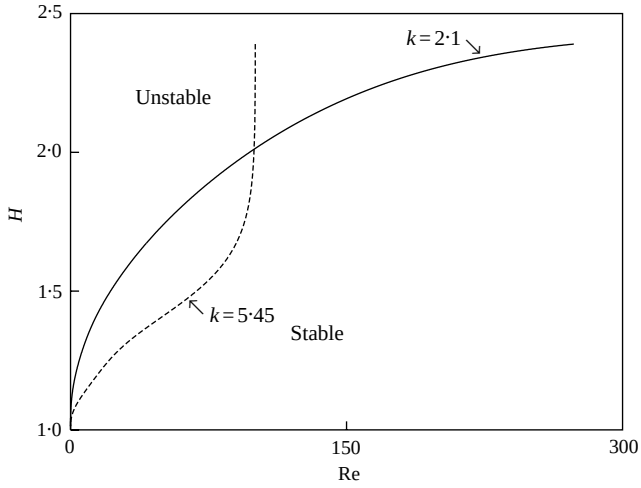

Figure 7. Neutral-stability curves in the (H, Re) plane for two different axial wavenumbers. Mode I instability; $\eta_r = 0$, $\Gamma = 8$, $n = 0$.

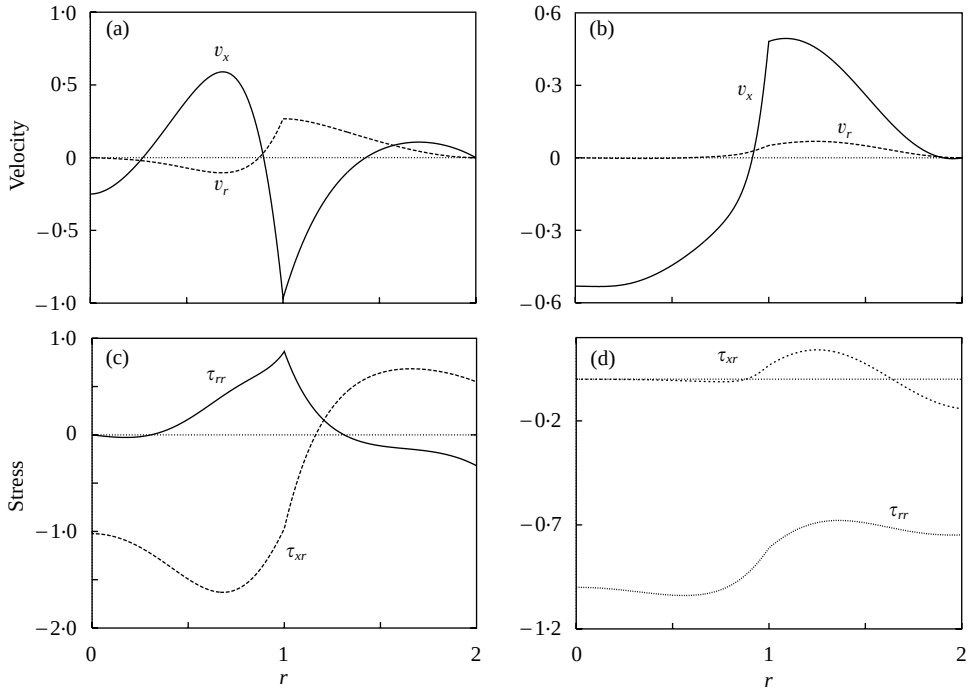

Figure 8. Radial profiles for the disturbance velocity and stress for the axisymmetric modes; $H = 2$, $\Gamma = 7$, Re = 23, $k = 2{\cdot}5$, $\eta_r = 0$. (a) Axial and radial disturbance velocities; Mode I. (b) Axial and radial disturbance velocities; Mode II. (c) Components of the viscous stress tensor; Mode I. (d) Components of the viscous stress tensor; Mode II. To preserve velocity continuity at the interface, we plot ($2\Gamma u_r + su_x$) for the axial velocity component in the solid medium ($r > 1$).

Depending on the fluid and wall parameters, the first instability to be observed may be axisymmetric ($n = 0$) or non-axisymmetric ($n = 1, 2, \ldots$). Figure 10 shows the neutral-stability curves in the (Γ, Re)-plane for different modes and azimuthal wavenumbers. The

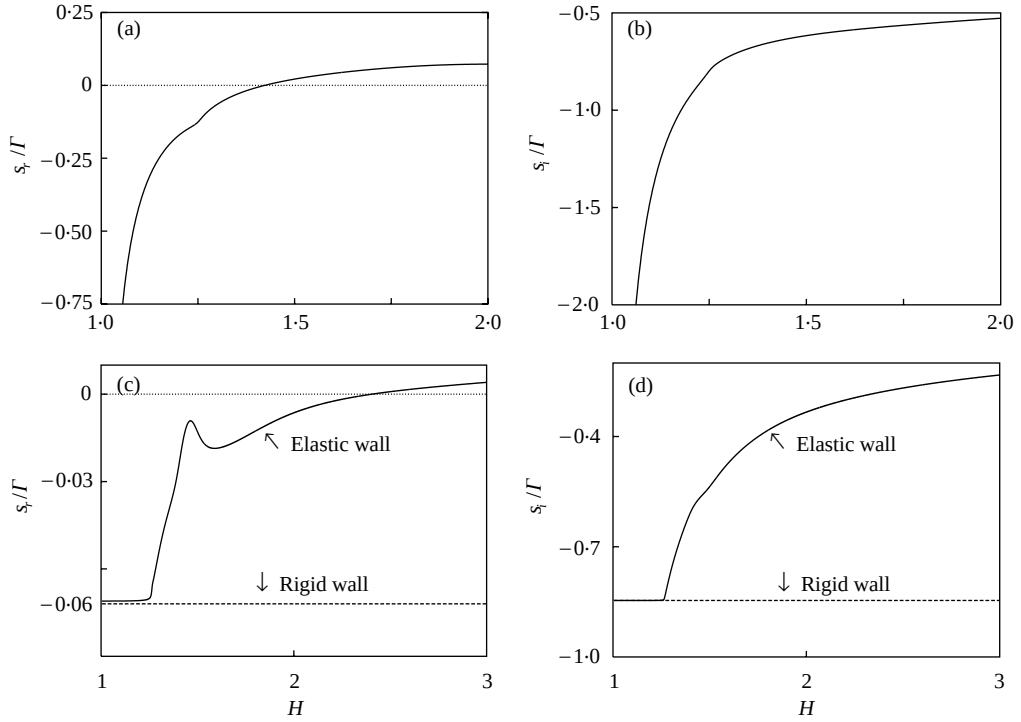

Figure 9. Real and imaginary parts of s/Γ for the non-axisymmetric unstable modes versus the depth of the elastic material; $\Gamma = 7$, $n = 1$, $\eta_r = 0$, $k = 1$, Re = 1000. (a) Mode III real part. (b) Mode III imaginary part. (c) Mode IV real part. (d) Mode IV imaginary part.

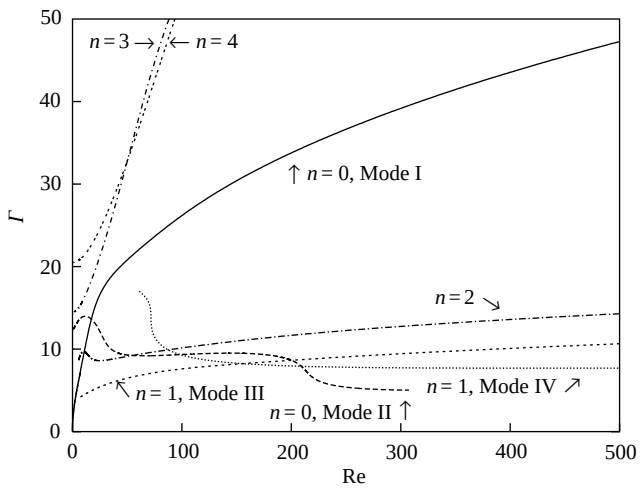

Figure 10. Neutral-stability curves in the plane (Γ, Re) for different modes and different values of n; $H = 2, k = 0{\cdot}5, \eta_s = 0$. The region below each indicated neutral-stability curve is stable and that above each curve is unstable.

region below each curve is stable and above each curve is unstable. All the modes are stable at sufficiently low Γ, which is expected because, for a given Re, the shear modulus G goes to infinity when Γ goes to zero. The coating is stiffer and hence stable at low Γ. When

Γ increases to a value above the neutral curve, the coupled system becomes unstable. The stable regions are bounded by the Re-axis and the respective neutral curves, which in the order of increasing Reynolds number are stable regions for Mode I, Mode III, Mode IV, and finally Mode II. As an example, at the point (Γ, Re) = (10, 100), Mode III is unstable while Mode I is stable. For a given Reynolds number, the non-axisymmetric mode with $n = 1$ first becomes unstable as the coating becomes softer, followed by the non-axisymmetric modes with $n = 2$, 3 and 4. Again for a given Re, the axisymmetric Mode I becomes unstable at higher values of Γ as compared to the non-axisymmetric modes with $n = 1$ and 2, but at lower values of Γ as compared to the non-axisymmetric modes with $n = 3$ and 4.

For the parameters considered in Figure 10, the system is most unstable for the axisymmetric modes for low and high Reynolds numbers and the non-axisymmetric modes for intermediate Reynolds numbers. The axisymmetric and non-axisymmetric modes observed to be the first unstable modes at low Reynolds number are Mode I and Mode III, while the axisymmetric and non-axisymmetric modes selected at high Reynolds number are Mode II and Mode IV. As will be shown later, however, for values of the Reynolds number higher than those considered in Figure 10, Mode I, Mode II and Mode IV become stable for both azimuthal wavenumbers $n = 0$ and 1, while the non-axisymmetric Mode III remains unstable. Thus, for a high Reynolds number, say $\mathrm{Re} > 1000$, the non-axisymmetric Mode III with the azimuthal wavenumber $n = 1$ is the sole unstable mode.

Figure 10 also shows that for $\mathrm{Re} < 50$, the non-axisymmetric mode with azimuthal wavenumber $n = 3$ becomes unstable at lower values of Γ than the non-axisymmetric mode with azimuthal wavenumber $n = 4$. This trend is reversed for $\mathrm{Re} > 50$. Consequently, it is difficult to predict from this result the shape of the neutral-stability curves for large values of n where there may exist other kinds of instabilities as was shown in the inviscid calculations of Kumaran (1996).

Figure 11 shows the neutral-stability curves in the plane (k, Re) for different values of Γ. The curves labelled $\Gamma = 7$ and 8 each has two branches. The lower branch is associated with the non-axisymmetric Mode III, while the top branch is associated with Mode IV instability. For $\Gamma \geq 9$, the two branches do not meet and we plotted only the respective lower branch.

The effect of increasing the depth of the viscoelastic material is to destabilize the system to non-axisymmetric modes, as shown in Figure 12 where Mode IV neutral-stability curves in the plane (H, Re) are plotted for two values of the axial wavenumber and two values of the viscosity of the coating. Furthermore, Figure 12 shows that the instabilities introduced by the high-wavenumber (short-wavelength) modes are limited to the low-Reynolds-number regime. Both of these results are qualitatively similar to the axisymmetric modes results discussed in Section 4.1. Figure 12 also indicates the effect of the viscosity ratio η_r on the stability of the system. Note that increasing the viscosity of the viscoelastic medium slightly changes the stability of the system. The instability of Mode IV seems to be weakly affected by the irreversible processes in the solid, which is characteristic of class C waves discussed in Section 1.3.

Figure 13 shows typical radial profiles for the disturbance velocity and stress. This is shown for the non-axisymmetric Mode III and Mode IV instabilities, both having the azimuthal wavenumber $n = 1$. The amplitude of the radial velocity component is small when compared to the axial velocity component at the interface between the fluid and compliant coating, as seen in Figures 13(a,b). Furthermore, the axial velocity component dominates the entire fluid and solid media instead of being confined to a thin region near the interface, as is the case in a rigid-walled tube. For Mode III, the energy production by the Reynolds stress, $-v_r v_x \, \mathrm{d}v/\mathrm{d}r$, is negative in a narrow region near the wall but is predominately positive in the rest of the fluid region, as can be seen in Figure 13(a), so that

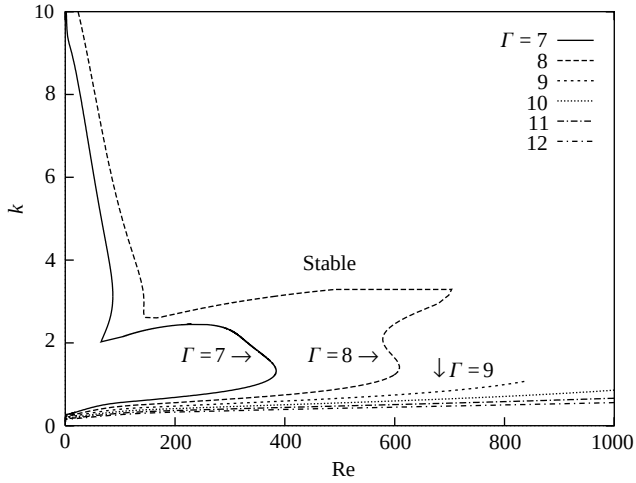

Figure 11. Neutral-stability curves in the plane (k, Re) for different values of Γ; $H = 2$, $n = 1$, $\eta_s = 0$. Mode III and Mode IV instabilities.

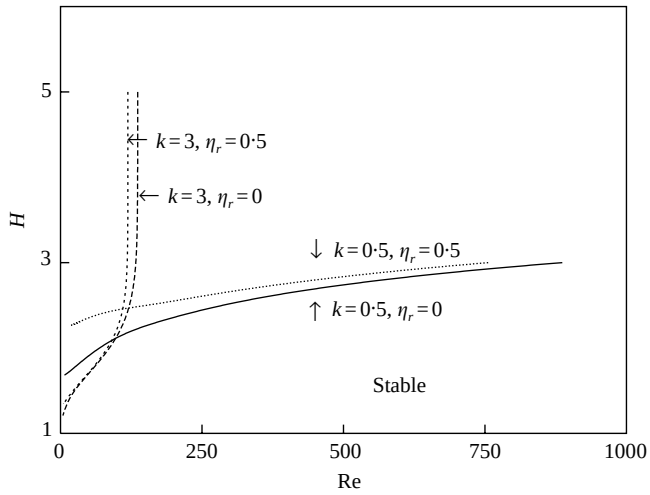

Figure 12. Effect of dissipation in the solid and axial wavenumber on the neutral-stability curves in the plane (H, Re). Mode IV instability; $n = 1$, $\Gamma = 7$.

the Reynolds stress tends to destabilize the disturbance. It will be shown in the following section that the energy of Mode III disturbance is produced by both the Reynolds stress and by the work of the viscous shear stress at the interface. For Mode IV, the energy production by the Reynolds stress is negative [Figure 13(b)], which stabilizes this mode.

5. ENERGY CONSIDERATIONS

In this section, we consider the energy transfer between the fluid and compliant media. Let $\varphi(r, \theta, x, t) = 0$ be the equation of the interface. The function φ may be expanded in the vicinity of the equilibrium position at $r = 1$, this leads to

$$\varphi(1, \theta, x, t) + (r - 1)d_r\varphi + \mathcal{O}[(r - 1)^2] = 0. \tag{58}$$

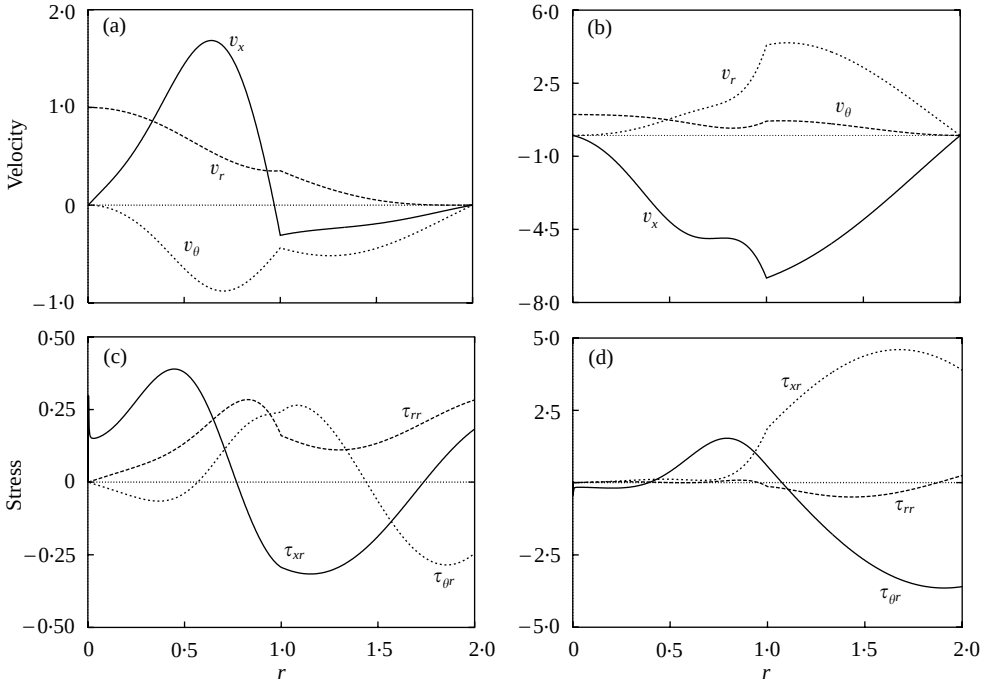

Figure 13. Radial profiles for the disturbance velocity and stress for the non-axisymmetric modes; $H = 2$, $\Gamma = 7$, $\mathrm{Re} = 100$, $k = 1$, $n = 1$, $\eta_r = 0$. (a) Axial, radial and azimuthal velocities; Mode III. (b) Axial, radial and azimuthal velocities; Mode IV. (c) Components of the viscous stress tensor; Mode III. (d) Components of the viscous stress tensor; Mode IV. To preserve velocity continuity at the interface, we plot $(2\Gamma u_r + su_x)$ for the axial velocity component in the solid medium ($r > 1$).

For an infinitesimal disturbance, the previous equation is reduced to

$$r = 1 - \phi(\theta, x, t), \tag{59}$$

where at $r = 1$,

$$\phi(\theta, x, t) = \frac{\varphi(1, \theta, x, t)}{d_r \varphi(1, \theta, x, t)}. \tag{60}$$

It follows that the outward normal at the interface is given by

$$\mathbf{n} = \left(d_r, \frac{\partial_\theta}{r}, \partial_x\right)[r - 1 + \phi(\theta, x, t)] = \left(1, \frac{\partial_\theta \phi}{r}, \partial_x \phi\right). \tag{61}$$

For brevity, we write

$$\mathbf{n} = \left(1, \frac{\partial_\theta \phi}{r}, \partial_x \phi\right) = (1, \alpha, \beta), \tag{62}$$

where α, β are infinitesimal quantities. The force applied by the elastic medium on the side of the surface element ds located at the interface is

$$\mathrm{d}\mathbf{F} = \boldsymbol{\sigma} \cdot \mathbf{n}\, \mathrm{d}s, \tag{63}$$

where σ is the stress tensor. Through the surface element ds, the elastic medium receives the infinitesimal energy quantity

$$\mathrm{d}p = -\, d\mathbf{F}\cdot\partial_t\mathbf{u}\,\mathrm{d}s = -\,(\boldsymbol{\sigma}\cdot\mathbf{n})\cdot\partial_t\mathbf{u}\,\mathrm{d}s, \tag{64}$$

where $\partial_t\mathbf{u}$ is the velocity of a solid particle at the interface. Expansion of the stress term gives

$$(\sigma\cdot\mathbf{n})\cdot\partial_t\mathbf{u} = \partial_t u_r(\sigma_{rr} + \alpha\sigma_{r\theta} + \beta\sigma_{rx}) + \partial_t u_\theta(\sigma_{\theta r} + \alpha\sigma_{\theta\theta} + \beta\sigma_{\theta x}) + \partial_t u_x(\sigma_{xr} + \alpha\sigma_{x\theta} + \beta\sigma_{xx}). \tag{65}$$

All the derivatives in the above equation are computed at $r = 1$. Moreover, the terms that contain α or β may be neglected in the linear theory, so that the energy flux from the fluid to the solid through the interface surface S may be written as

$$P_s = -\iint(\sigma_{rr}\partial_t u_r + \sigma_{\theta r}\partial_t u_\theta + \sigma_{xr}\partial_t u_x)\,\mathrm{d}s. \tag{66}$$

Here, $r = 1$, $\mathrm{d}s = (\mathrm{d}x\,\mathrm{d}\theta)$, $0 \le \theta \le 2\pi$, and $0 \le x \le 2\pi/k$. Owing to the fact that the disturbance is a normal mode, the integral in equation (66) leads to

$$P_s = \frac{-\,4\pi^2\mathrm{e}^{2s_r t}[s(\tilde{u}_r\tilde{\sigma}^*_{rr} + \tilde{u}_\theta\tilde{\sigma}^*_{\theta r} + \tilde{u}_x\tilde{\sigma}^*_{xr}) + \mathrm{cc}]}{nk}, \tag{67}$$

where the * superscript indicates a complex conjugate. Of course, when the instabilty mode is axisymmetric, the above expression becomes

$$P_s = \frac{-\,4\pi^2\mathrm{e}^{2s_r t}[s(\tilde{u}_r\tilde{\sigma}^*_{rr} + \tilde{u}_x\tilde{\sigma}^*_{xr}) + \mathrm{cc}]}{k}. \tag{68}$$

Due to the fact that there is no energy source in an elastic medium, the growth of an unstable mode in such a medium must be due to the energy flux from the flowing fluid toward the elastic solid. Thus, when the mode is unstable, the energy flux toward the elastic medium must be positive. For both the axisymmetric Mode I and Mode II waves, Figure 14 shows the effects of the coating thickness and the Reynolds number on the energy flux from the flowing fluid to the solid medium and the amplification rate. A comparison is made in the figure between an elastic coating (E) and a viscoelastic (V) one. The same quantities are plotted in Figure 15 for the azimuthally varying Mode III and Mode IV disturbances. As can be seen, the energy flux and the amplification rate have the same algebraic sign when the wall is elastic.

The above argument can be better understood from the energy balance equation for the fluctuating component of the disturbance in the solid

$$d_t E_s = P_s - D_s, \tag{69}$$

where E_s is the energy of the solid, P_s is the deformation work due to the stress at the fluid–solid interface, and D_s is the rate of energy dissipation due to the solid viscosity. The energy flux due to the work of the streamwise, radial and azimuthal stress were computed by Hamadiche (1999*a*, *b*) and compared to the rate of amplification and the total energy transfer. It was found that the energy transfer to the solid is mostly due to the work of the shear stress at low Reynolds numbers, say, $\mathrm{Re} < 100$, but is mostly due to the normal stress at high Reynolds numbers. However, at high Reynolds numbers, the work done by the radial stress is almost balanced by that done by the shear stress and the small difference between the two determines the stability or instability of the system. This can be seen for Mode II instability in Figure 16, reproduced from Hamadiche (1999*a*).

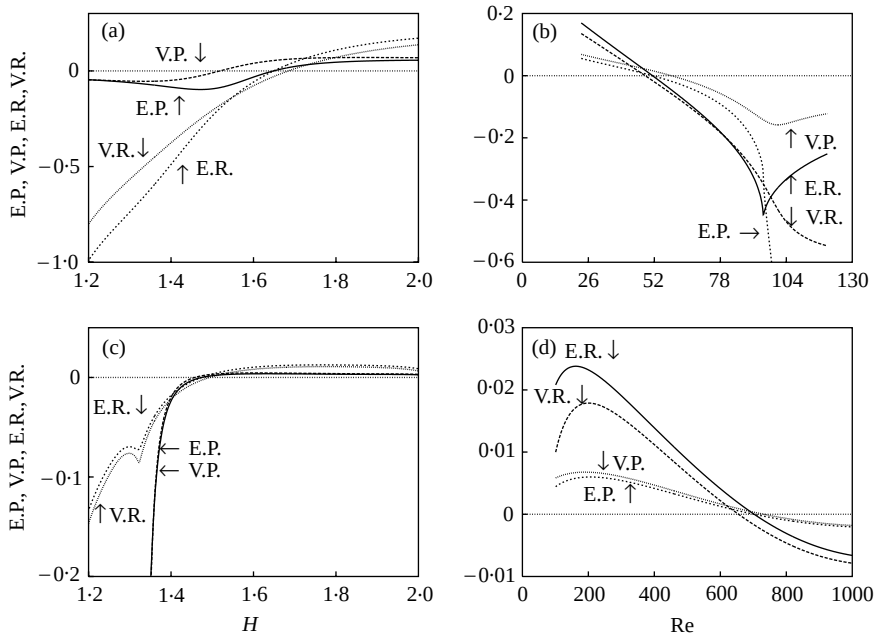

Figure 14. Variation of energy flux toward the compliant coating and the amplification rate with the depth of the pliable material and the Reynolds number for the axisymmetric modes. E: elastic wall, $\eta_r = 0$; V: viscoelastic wall, $\eta_r = 0{\cdot}3$; R: amplification rate; P: power. (a) Mode I; $\Gamma = 6$, $k = 2{\cdot}5$, Re = 23. (b) Mode I; $\Gamma = 6$, $k = 2{\cdot}5$, $H = 2$. (c) Mode II; $\Gamma = 6$, $k = 1$, Re = 500. (d) Mode II; $\Gamma = 6$, $k = 1$, $H = 2$.

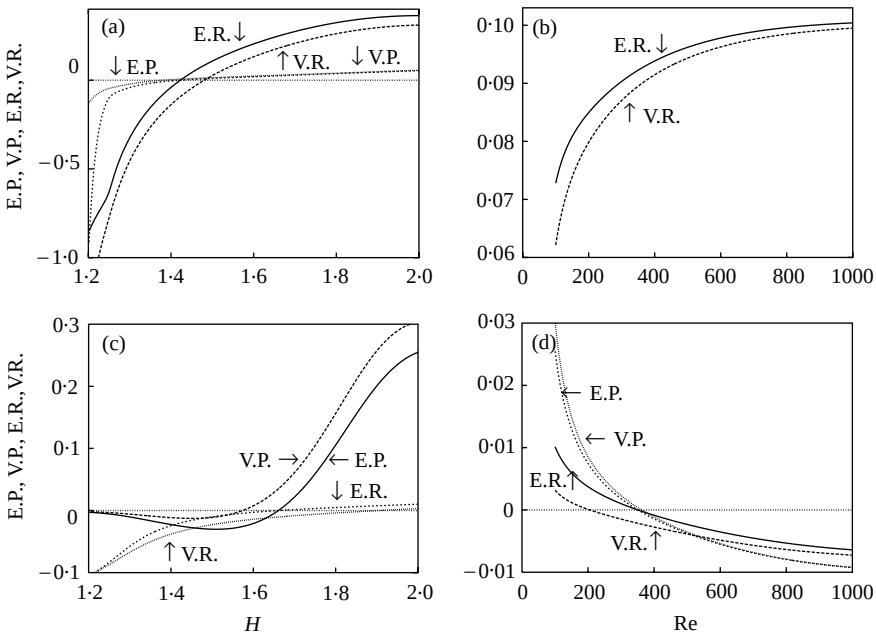

Figure 15. Variation of energy flux toward the compliant coating and the amplification rate with the depth of the pliable material and the Reynolds number for the non-axisymmetric modes; $\Gamma = 7$, $k = 1$. E: elastic wall, $\eta_r = 0$; V: viscoelastic wall, $\eta_r = 0{\cdot}3$; R: amplification rate; P: power. (a) Mode III; Re = 100. (b) Mode III; $H = 2$. (c) Mode IV; Re = 100. (d) Mode IV; $H = 2$.

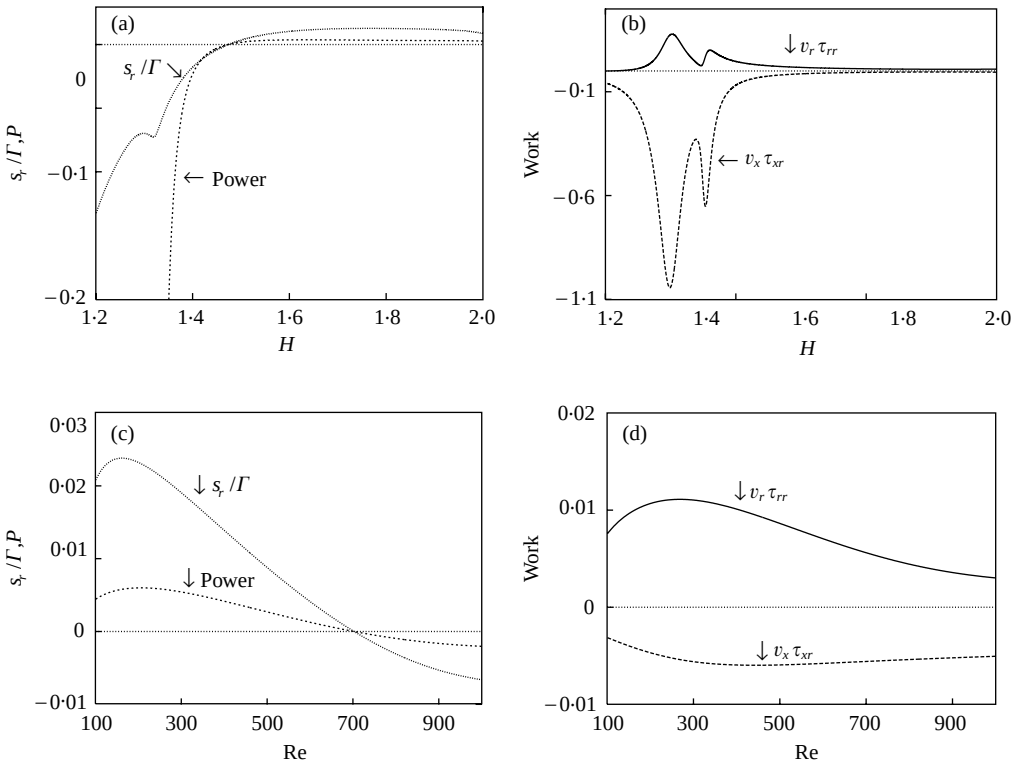

Figure 16. Variation of energy flux toward the compliant coating, the amplification rate and the work done by the stress at the interface with the depth of the pliable material and the Reynolds number; Mode II instability, $\Gamma = 6$, $k = 1$, $n = 0$, $\eta_r = 0$. (a) Power and amplification rate; Re = 500. (b) Work done by the stress; Re = 500. (c) Power and amplification rate; $H = 2$. (d) Work done by the stress; $H = 2$. Reproduced from Hamdiche (1999*a*).

It is important to note that the stability of the system at high Reynolds numbers is due to the fact that the shear stress component returns to the fluid a quantity of energy greater than the energy supplied to the solid by the radial stress component. It can be concluded from the work of Hamadiche (1999*a*, *b*) that the energy transfer, at high Reynolds numbers, is essentially due to the work done by the radial stress component, even though this term does not contribute to the total energy of the disturbance. The azimuthal and shear stress components often have a stabilizing effect at high Reynolds numbers.

The energy balance equation equation (69) does not display the energy transfer from the mean flow to the disturbance. This can be seen from the equation representing the total system energy (Chandrasekhar 1981). Using Kumaran's (1995*b*) notations, such an equation can be written in the following simple form:

$$d_t E = C + S - D, \tag{70}$$

where E is the total energy of the system, C is the rate of the energy production by the Reynolds stress terms, S is the deformation work due to the shear stress at the interface, and D is the rate of dissipation of energy in the fluid and in the solid. Owing to the discontinuity of the velocity of the disturbance at the interface, we have

$$S = P_s + P_f = \iint [(v_x - \partial_t u_x)\sigma_{xr}]_{r=1}\,\mathrm{d}s, \tag{71}$$

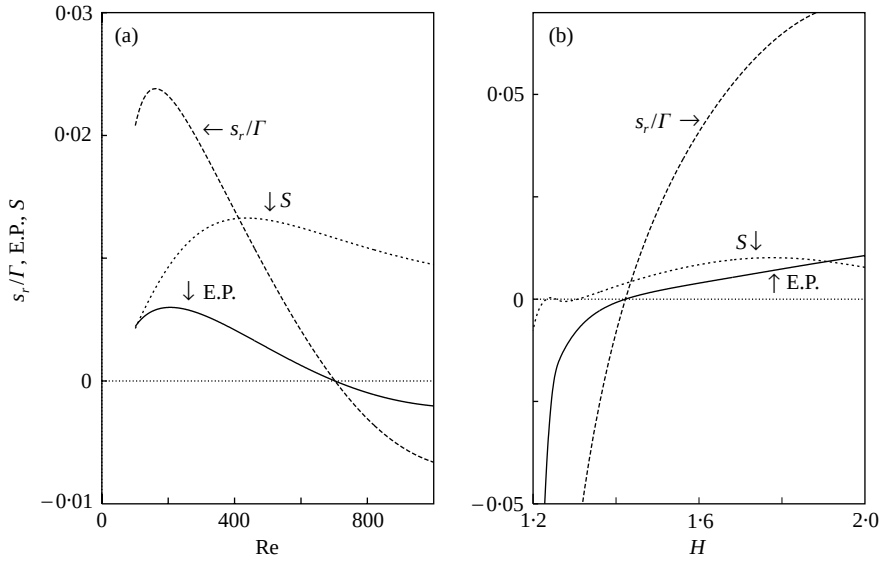

Figure 17. Comparison between the amplification rate, the total energy flux through the interface and the net work done by the shear stress at the interface; $\eta_r = 0{\cdot}0$, $k = 1$. E.P.: elastic power; S: net work done by the viscous shear stresses at the interface. (a) Mode I; $n = 0$, $\Gamma = 6$, $H = 2$. (b) Mode III; $n = 1$, $\Gamma = 7$, Re = 100.

where P_f is the work done on the fluid at the interface. For both Mode I and Mode III, Figure 17 shows the deformation work due to the shear stress at the interface and a comparison with the rate of amplification and the total energy flux toward the solid. As can be seen, the axisymmetric Mode I becomes stable even though the deformation work S is positive. In fact, the deformation work at the interface in this case is set off by the work done by the Reynolds stress which is negative. Thus, the Reynolds stress stabilizes the system when the disturbance is Mode I. For the non-axisymmetric Mode III, however, the work done by the stress at the interface is positive only when the mode is unstable, as shown in Figure 17(b). Figure 13 previously showed that the work done by the Reynolds stress, C, is also positive, so that Mode III is destabilized by both the deformation work at the interface and by the Reynolds stress.

6. DISCUSSION AND CONCLUDING REMARKS

In the present study, the stability of the incompressible Hagen–Poiseuille flow of a Newtonian fluid in a compliant tube contained within a rigid, hollow cylinder was determined using linear stability analysis. The wall was modelled as a homogeneous, incompressible, viscoelastic medium, where the stress has an elastic component proportional to the strain and a viscous component proportional to the strain rate. The dynamics of the system is influenced by four dimensionless parameters: the Reynolds number $\mathrm{Re} = (\rho V R/\eta)$; the ratio of radii H; the ratio of the viscosities of the wall material and the fluid $\eta_r = (\eta_s/\eta)$; and the dimensionless velocity $\Gamma = (\rho V^2/G)^{1/2}$.

The linear stability theory was used to examine the temporal stability of the described system subjected to infinitesimal axisymmetric or non-axisymmetric disturbances. Once the nonlinear terms were neglected, the resulting partial differential equations were transformed into a system of first-order differential equations. This system was numerically integrated using a fourth-order Runge–Kutta algorithm. The boundary conditions at the interface lead

to an eigenvalue problem. Using Cauchy's theorem, the eigenvalues lying within a circle $|s| = a$ in the complex s-plane were found, where the center of the circle is located at the origin of the complex plane. The present procedure allows for a good initial condition, without guess, to a Newton–Raphson algorithm which readily converges to the more accurate eigenvalues. Furthermore, the continuation method was used to find the eigenvalues for new values of the four dimensionless control parameters. In order to validate our numerical method, we compared the present results with the results of Kumaran (1995*a*) and the results of Salwen & Grosch (1972) and Gill (1973). The agreement between ours and their results is very good.

We examined in more detail the unstable modes obtained with the two azimuthal wavenumbers $n = 0$ and 1. For $n = 0$, we found two unstable axisymmetric modes which we termed Mode I and Mode II. For $n = 1$, there are two unstable non-axisymmetric modes: Mode III and Mode IV. We found that for high Reynolds numbers, only Mode III persists. When the depth of the viscoelastic layer goes to zero, Mode II and Mode IV asymptote to the least-damped modes of Hagen–Poiseuille flow in a rigid-walled tube, while Mode I and Mode III become extremely stabilized. It is thus concluded that Mode II and Mode IV are fluid-based instabilities, while Mode I and III are solid-based, flow-induced surface instabilities.

The effect of the compliant-wall viscosity was examined. It was found that wall dissipation damps, to different degrees, all four unstable modes. This suggests that these modes do not belong to class A, introduced by Benjamin (1963). For all four unstable modes, we plot in Figure 18 the group velocity and amplification rate as functions of the wavenumber. Mode I has a significant positive group velocity, although consistently lower than the mean

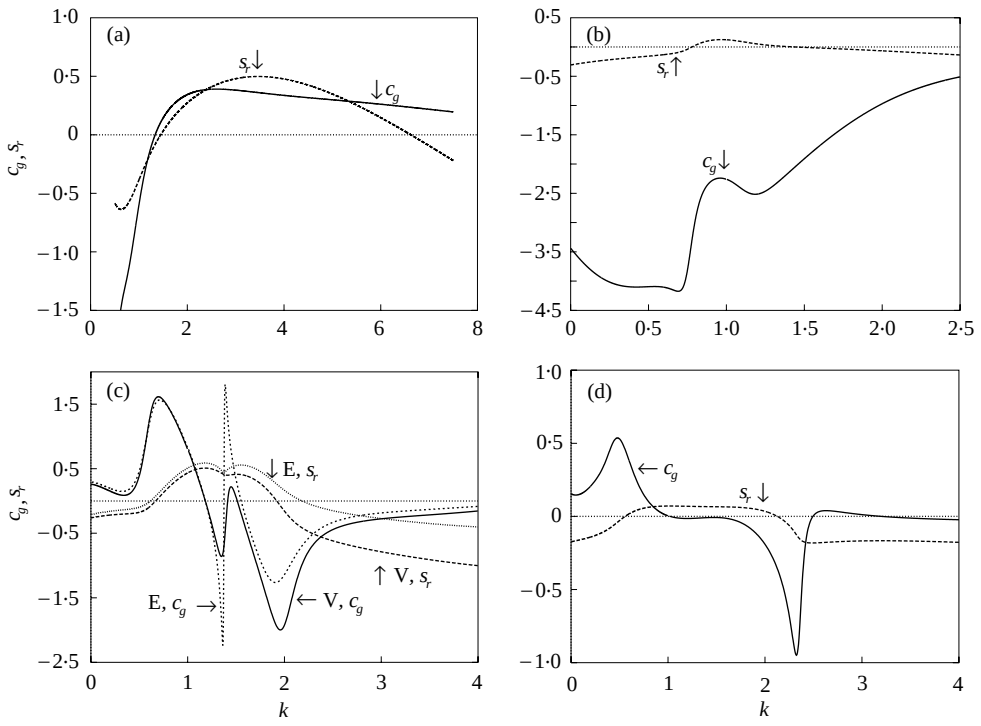

Figure 18. Group velocity c_g and amplification rate versus the wavenumber. E: elastic wall, $\eta_r = 0$; V: viscoelastic wall, $\eta_r = 0{\cdot}3$. (a) Mode I; $\Gamma = 6$, $H = 2$, $k = 2{\cdot}5$, $n = 0$, Re = 23. (b) Mode II; $\Gamma = 6$, $H = 2$, $k = 1$, $n = 0$, Re = 100. (c) Mode III; $\Gamma = 7$, $H = 2$, $k = 1$, $n = 1$, Re = 100. (d) Mode IV; $\Gamma = 7$, $H = 2$, $k = 1$, $n = 1$, Re = 100.

TABLE 1
Summary of all four instability modes

	Mode I	Mode II	Mode III	Mode IV
Symmetry	Axisymmetric	Axisymmetric	Non-axisymmetric	Non-axisymmetric
Base	Solid-based	Fluid-based	Solid-based	Fluid-based
n	0	0	1, 2, 3, …	1, 2, 3, …
$(H-1)\ll 1$	Diverge	Least-damped rigid-wall mode	Diverge	Least-damped rigid-wall mode
$\mathrm{Re}\gg 1$	Stable	Stable	Unstable	Stable
c_g	Positive	Negative	Positive for small k Negative for large k	Nearly zero
Solid viscosity	Stabilizing	Stabilizing	Stabilizing	Stabilizing

flow velocity at the center of the tube. It may thus be inferred that the solid-based, axisymmetric Mode I is a flutter mode and belongs to class B. Mode II has a significant negative group velocity which is higher than the velocity of the mean flow at the center of the tube. The group velocity of Mode III is positive for low wavenumbers (long wavelengths) and negative for high wavenumbers. The non-axisymmetric Mode III is very dispersive. The group velocity of Mode IV is close to zero for most of the range of unstable wavenumbers. This suggests that Mode IV, though fluid-based, is a standing-wave divergence instability belonging to class C. An examination of the spatio-temporal instability, along the lines described by Yeo *et al.* (1996, 1999) for a boundary layers, is required in order to reveal the presence of a pinch point in the Fourier contour and thus to confirm the absolute nature of Mode IV instability. Table 1 summarizes the properties of Mode I–Mode IV instabilities.

An inspection of the energy balance equation related to the viscoelastic wall shows that the system is unstable when the energy flux is from the fluid to the wall. The energy flux from the flowing fluid to the viscoelastic wall across the interface was numerically computed and compared to the amplification rate. It was found that the system is unstable (stable) when the energy flux is from (to) the fluid to (from) the viscoelastic medium. The power developed by each force component at the interface was computed. It was found that at high Reynolds numbers, the energy transfer from the fluid to the solid is mostly done by the work of the component of the stress perpendicular to the wall (pressure force), while the tangential stress plays a more important role at low Reynolds numbers.

Examination of the total energy balance for the coupled system showed that the fluid-based disturbance energy is produced, to different degrees, by the work of the viscous shear stress at the interface between the fluid and the solid and the Reynolds stress in the fluid. Computation of the work done by the shear stress at the interface and the velocity of the disturbance showed that the energy of the unstable axisymmetric Mode I and non-axisymmetric Mode IV is produced by the work of the shear stress at the interface, while the Reynolds stress tends to stabilize these disturbances. On the other hand, the energy of the unstable axisymmetric Mode II and non-axisymmetric Mode III is produced by both the Reynolds stress and the shear stress at the interface. Thus, the Reynolds stress seems to have a stabilizing effect on Mode I and IV but a destabilizing effect on Mode II and Mode III.

The effect of the thickness of the viscoelastic material was also examined. Since the displacement of the wall at $r = H$ is restricted by the boundary condition applied at the rigid wall, the system is expected to be stable for small values of $(H-1)$. In fact, it was

shown that the coupled system is stable when the depth of the viscoelastic material is very small ($H = 1{\cdot}05$). Moreover, it was found that Mode II and Mode IV tend to the least-damped modes in a rigid-walled tube, while Mode I and Mode III diverge when $H \to 1$ (depth of coating goes to zero). The effect of increasing H from 1 is to destabilize the system.

The effect of Reynolds number was also examined. Putting aside the effect of the other control parameters, it was found that Mode I, Mode II and Mode IV become stable at high Reynolds numbers, while Mode III remains unstable at high Reynolds numbers. It was shown that the most excited mode may be an axisymmetric or non-axisymmetric one according to the values of several parameters. We found that when the Reynolds number is close to zero, the first excited mode is the axisymmetric Mode I. When the Reynolds number increases, the non-axisymmetric Mode IV with an azimuthal wavenumber $n = 1$ becomes the most unstable mode. By further increasing the Reynolds number, the previous mode is replaced by the non-axisymmetric Mode III with an azimuthal wavenumber $n = 1$. For larger values of the Reynolds number, the first excited mode is the axisymmetric Mode II.

The unstable axisymmetric and non-axisymmetric eigenfunctions were plotted versus the radial coordinate r. As intuitively expected, it was found that the radial velocity component is small in comparison to the streamwise and azimuthal velocity components. The streamwise and azimuthal velocity components are, however, of the same order of magnitude. The form of the unstable disturbance shows that the Reynolds stress tends to stabilize the unstable non-axisymmetric Mode IV when the instability takes place at low Reynolds numbers and the energy of the disturbance is supplied by the deformation work done at the interface. The form of the unstable non-axisymmetric Mode III shows that the Reynolds stress tends to destabilize the system and, together with the deformation work, supplies energy to the unstable mode.

The low-Reynolds-number Mode I instability whose growth is energized only by the work of the viscous shear stress at the fluid–solid interface is perhaps related in physical origin to the surface-shear-dominated instability termed B_2 mode by Yeo (1988) who identified it while investigating the stability of the canonical boundary layer flow over the same type of compliant coating analyzed here. Yeo's mode would occur in the developing region of a pipe flow and might be the natural precursor to Mode I instability in the fully developed region. Although the B_2 instability mode may not exist right down to zero Reynolds number for a boundary layer due to the strong divergence of the mean flow in that regime, the instability can exist to significantly high Re and may even merge or coalesce with other instabilities as the surface becomes highly compliant, producing perhaps the like of the coalescence Mode IV identified in our investigation.

In the present formulation, we neglected the effect of pressure gradient along the undisturbed flow on the compliant wall deformation. Owing to this favorable pressure-gradient, the deformation would increase along the tube, thus slightly reducing the effective tube radius R. A variable-radius pipe is a challenging, spatially inhomogeneous problem which we defer to another study, and the radius R was taken as constant in the present formulation.

The results described here should be useful when designing a compliant coating to effect certain beneficial flow-control goals in man-made pipe flows. The present stability analysis is linear, but extending the present exercise to nonlinear stability calculations may be a useful next step. Finally, applying the compliant tube studies to the understanding of bodily fluid flows in various biological systems is certainly a worthwhile endeavor.

References

BENJAMIN, T. B. 1963 The threefold classification of unstable disturbances in flexible surfaces bounding inviscid flows. *Journal of Fluid Mechanics* **16,** 436–450.

BUSHNELL, D. M., HEFNER, J. N. & ASH, R. L. 1977 Effect of compliant wall motion on turbulent boundary layers. *Physics of Fluids* **20,** (Part II), S31–S48.

CARPENTER, P. W. 1988 The optimization of compliant surfaces for transition delay. In *Turbulence Management and Relaminarisation* (eds H. W. Liepmann & R. Narasimha), pp.–313. Berlin: Springer-Verlag.

CARPENTER, P. W. 1990 Status of transition delay using compliant walls. In *Viscous Drag Reduction in Boundary Layers* (eds D. M. Bushnell & J. N. Hefner), pp. 79–113. Washington, DC: AIAA.

CARPENTER, P. W. 1993 Optimization of multiple-panel compliant walls for delay of laminar-turbulent transition. *AIAA Journal* **31,** 1187–1188.

CARPENTER, P. W. 1998 Current status of the use of wall compliance for laminar-flow control. *Experimental Thermal and Fluid Science* **16,** 133–140.

CARPENTER, P. W. & GAJJAR, J. S. B. 1990 A general theory for two- and three-dimensional wall-mode instabilities in boundary layers over isotropic and anisotropic compliant walls. *Theoretical and Computational Fluid Dynamics* **1,** 349–378.

CARPENTER, P. W. & GARRAD, A. D. (1985) The hydrodynamic stability of flow over Kramer-type compliant surfaces. Part 1. Tollmien–Schlichting instabilities. *Journal of Fluid Mechanics* **155,** 465–510.

CARPENTER, P. W. & GARRAD, A. D. (1986) The hydrodynamic stability of flow over Kramer-type compliant surfaces. Part 2. Flow-induced surface instabilities. *Journal of Fluid Mechanics* **170,** 199–232.

CHANDRASEKHAR, S. 1981 *Hydrodynamic and Hydromagnetic Stability*. New York: Dover.

CORCOS, G. M. & SELLARS, J. R. 1959 On the stability of fully developed flow in a pipe. *Journal of Fluid Mechanics* **5,** 97–112.

DANIEL, A. P., GASTER, M. & WILLIS, G. J. K. 1987 Boundary layer stability on compliant surfaces. Final Report No. 35020, British Maritime Technology Ltd., Teddington, Great Britain.

DAVEY, A. & DRAZIN, P. G. 1969 The stability of Poiseuille flow in a pipe. *Journal of Fluid Mechanics* **36,** 209–218.

EVRENSEL, C. A., KHAN, M. R., ELLI, S. & KRUMPE, P. E. 1993 Viscous airflow through a rigid tube with a compliant lining: a simple model for the air–mucus interaction in pulmonary airways. *Journal of Biomechanical Engineering* **115,** 262–270.

GAD-EL-HAK, M. 1986*a* Boundary layer interactions with compliant coatings: an overview. *Applied Mechanics Reviews* **39,** 511–524.

GAD-EL-HAK, M. 1986*b* The response of elastic and viscoelastic surfaces to a turbulent boundary layer. *Journal of Applied Mechanics* **53,** 206–212.

GAD-EL-HAK, M. 1987 Compliant coatings research: a guide to the experimentalist. *Journal of Fluids and Structures* **1,** 55–70.

GAD-EL-HAK, M. 1996 Compliant coatings: a decade of progress. *Applied Mechanics Reviews* **49,** (Part 2), S1–S11.

GAD-EL-HAK, M. 2000 *Flow Control: Passive, Active, and Reactive Flow Management*. London: Cambridge University Press.

GAD-EL-HAK, M., BLACKWELDER, R. F. & RILEY, J. J. 1984 On the interaction of compliant coatings with boundary layer flows. *Journal of Fluid Mechanics* **140,** 257–280.

GARG, V. K. & ROULEAU, W. T. 1972 Linear spatial stability of pipe Poiseuille flow. *Journal of Fluid Mechanics* **54,** 113–127.

GASTER, M. 1988 Is the dolphin a red herring? In *Turbulence Management and Relaminarisation* (eds H. W. Liepman & R. Narasimha), pp. 285–304. Berlin: Springer-Verlag.

GILL, A. E. 1973 The least-damped disturbance to Poiseuille flow in a circular pipe. *Journal of Fluid Mechanics* **61,** 97–107.

HAMADICHE, M. 1997 Stabilité de l'écoulement de Poiseuille en conduite viscoélastique cylindrique. In *Le troisième Congrès de Mécanique,* 23–25 Avril, Faculté des Sciences de Tétouan-Maroc, France.

HAMADICHE, M. 1998 Instabilité causée par l'interaction fluide/structure. In *34ème Colloque d'Aérodynamique Appliquée de la A.A.A.F.,* 23–25 Mars, ESM2, Marseille, France.

HAMADICHE, M. 1999*a* Flux d'énergie d'un écoulement de Poiseuille vers la paroi d'un tube élastique. a. Modes d'instabilité axisymetrique. *Comptes Rendus de l'Académie des Sciences Paris* **327,** Série IIb, 1155–1161.

HAMADICHE, M. 1999*b* Flux d'énergie d'un écoulement de Poisuille vers la paroi d'un tube élastique. b. Modes d'instabilité non axisymétrique. *Comptes Rendus de l'Académie des Sciences Paris* **327,** (Série IIb), 1163–1170.

HAMADICHE, M. & AL-FARKH, M. 1997 Stabilité linéaire de l'écoulement de Poiseuille en conduite cylindrique viscoélastique. *Comptes Rendus de l'Académie des Sciences Paris* **326** (Série IIb), 95–102.

HUERRE, P. & MONKEWITZ, P. A. 1990 Local and global instabilities in spatially developing flows. *Annual Review of Fluid Mechanics* **22,** 473–537.

KRAMER, M. O. 1957 Boundary-layer stabilization by distributed damping. *Journal of Aeronautical Sciences* **24,** 459–460.

KUMARAN, V. 1995*a* Stability of the viscous flow of a fluid through a flexible tube. *Journal of Fluid Mechanics* **294,** 259–281.

KUMARAN, V. 1995*b* Stability of the flow of a fluid through a flexible tube at high Reynolds number. *Journal of Fluid Mechanics* **302,** 117–139.

KUMARAN, V. 1996 Stability of an inviscid flow in a flexible tube. *Journal of Fluid Mechanics* **320,** 1–17.

KUMARAN, V. 1998*a* Stability of the flow of a fluid through a flexible tube at intermediate Reynolds number. *Journal of Fluid Mechanics* **357,** 123–140.

KUMARAN, V. 1998*b* Stability of wall modes in a flexible tube. *Journal of Fluid Mechanics* **362,** 1–15.

LANDAHL, M. T. 1962 On the stability of a laminar incompressible boundary layer over a flexible surface. *Journal of Fluid Mechanics* **13,** 609–632.

LANDAU, L. D. & LIFSHITZ, E. M. 1970 *Theory of Elasticity*. Translated from the Russian, second edition; Oxford: Pergamon Press.

LUCEY, A. D. & CARPENTER, P. W. 1993 The hydroelastic stability of three-dimensional disturbances of a finite compliant panel. *Journal of Sound and Vibration* **165,** 527–552.

LUCEY, A. D. & CARPENTER, P. W. 1995 Boundary layer instability over compliant walls: comparison between theory and experiment. *Physics of Fluids* **7,** 2355–2363.

METCALFE, R. W. 1994 Boundary layer control: a brief review. In *Computational Fluid Dynamics '94* (eds J. Periaux & E. Hirschel), pp. 52–60. New York: Wiley.

RILEY, J. J., GAD-EL-HAK, M. & METCALFE, R. W. 1988 Compliant coatings. *Annual Review of Fluid Mechanics* **20,** 393–420.

SALWEN, H. & GROSCH, C. E. 1972 The stability of Poiseuille flow in a pipe of circular cross section. *Journal of Fluid Mechanics* **54,** 93–112.

SEN, P. K. & ARORA, D. S. 1988 On the stability of laminar boundary-layer flow over a flat plate with a compliant surface. *Journal of Fluid Mechanics* **197,** 201–240.

SHANKAR, V. & KUMARAN, V. 1999 Stability of non-parabolic flow in a flexible tube. *Journal of Fluid Mechanics* **395,** 211–236.

SHANKAR, V. & KUMARAN, V. 2000 Stability of fluid flow in a flexible tube to non-axisymmetric disturbances. *Journal of Fluid Mechanics* **407,** 291–314.

WILLIS, G. J. K. 1986 Hydrodynamic stability of boundary layers over compliant surfaces. Ph.D. thesis, University of Exeter, Exeter, Great Britain.

YEO, K. S. 1988 The stability of boundary-layer flow over single- and multi-layer viscoelestic walls. *Journal of Fluid Mechanics* **196,** 359–408.

YEO, K. S., KHOO, B. C. & ZHAO, H. Z. 1996 The absolute instability of boundary-layer flow over viscoelestic walls. *Theoretical and Computational Fluid Dynamics* **8,** 237–252.

YEO, K. S., KHOO, B. C. & ZHAO, H. Z. 1999 The convective and absolute instability of fluid flow over viscoelastic compliant layers. *Journal of Sound and Vibration* **223,** 379–398.